How Big Can Supermassive BH Grow?

Omar López-Cruz

omarlx@inaoep.mx

Instituto Nacional de Astrofísca, Óptica y Electrónica (INAOE)
Sta. Ma. Tonantzintla, Puebla, México.

GH 2015:"Formation and Fueling of Supermassive Black Hole Seeds"
July 18, 2015

Collaborators

- Christopher Añorve (FACITE, Universidad de Sinaloa, México) First Licenciatura en Astronomía in México
- Mark Birkinshaw (Astrophysics, U Bristol, UK)
- Diana M. Worrall (Astrophysics, U Bristol, UK)
- Héctor J. Ibarra-Medel (INAOE, México, now at IA UNAM)
- Wayne A. Barkhouse (DPA, University of North Dakota, USA)
- Juan Pablo Torres-Papaqui (DAUG, México)
- Verónica Motta (DFA, U Valparaíso, Chile)

Outline

- I will try to pursue you that the known BH scaling law break down for cD galaxies (an special kind of BCG).

- And that the final BH masses might have been set by initial conditions.

1 kpc= 3.08521 X 10^{21} cm

DGCG: Driver for GALFIT on Cluster Galaxies

GALFIT fits two-dimensional surface brightness to galaxies on digital images.
GALFIT functions: Sérsic, exponential, Gaussian, King Profile, Nuker, PSF profiles.
DGCG adapts GALFIT (Peng et al. 2002) to cluster galaxies.

GALFIT ⟶

Añorve 2012, Ph.D. Thesis, INAOE.

Surface Brightness Models

E galaxies and bulges of S and S0 galaxies are well described by the Sérsic function Sérsic (1963):

$$I(R) = I_e \exp\left(-k\left[\left(\frac{R}{R_e}\right)^{1/n} - 1\right]\right) . \qquad (1)$$

Disks of S and S0 galaxies are well fitted by the exponential function de Vaucouleurs (1953)

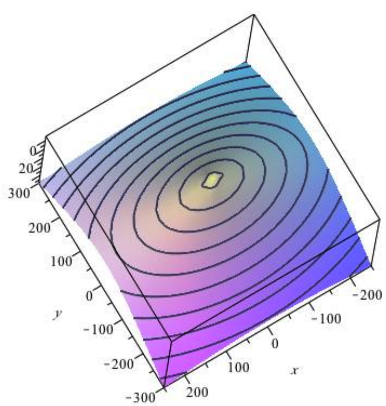

$$I(R) = I_0 \exp\left(-\frac{R}{R_s}\right) \qquad (2)$$

$$R = \left(x^{c+2} + \left(\frac{y}{q}\right)^{c+2}\right)^{\frac{1}{c+2}}$$

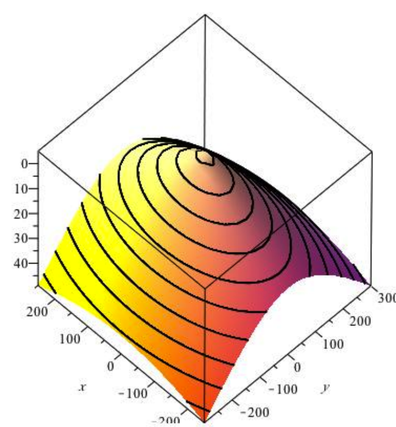

Surface Brightness Models

Strategy: Fit Sérsic (SS) and Sérsic + Exponential (BD) surface brightness to cluster galaxies

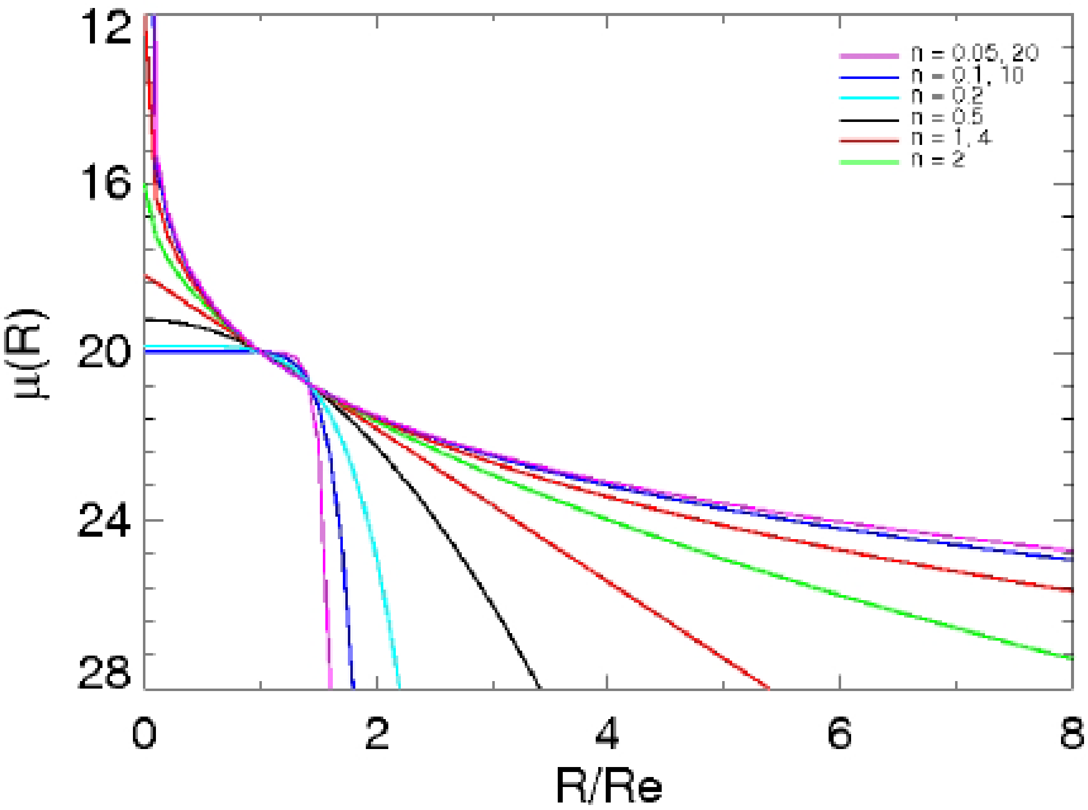

DGCG: Algorithm

1. Initial parameters (SExtractor; Bertin & Arnouts 1996)
2. Masking & Sky
3. Sorting
4. Fitting - Single, simultaneous
5. Bumpiness

DGCG: Algorithm

1.- Reads SExtractor catalog (Bertin & Arnouts 1996)

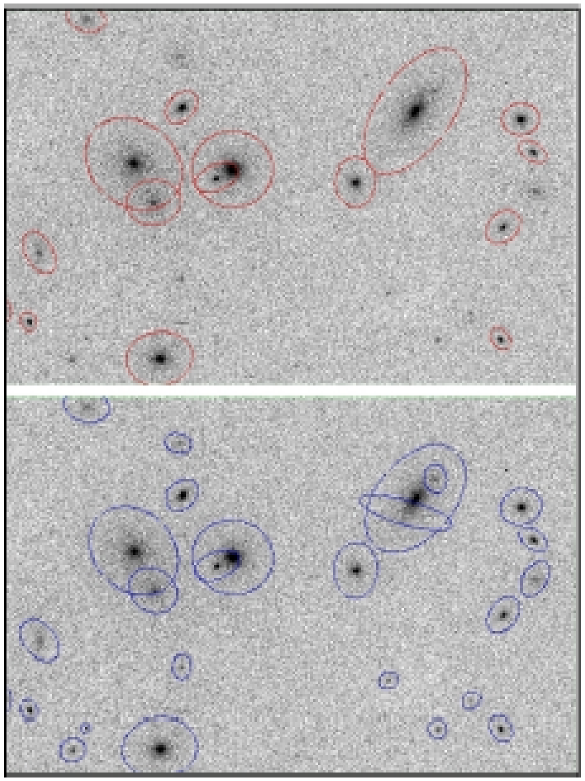

Star/Galaxy Classification (PPP)

DGCG: Algorithm

2.- Creates Mask and computes Sky for every object on the catalog

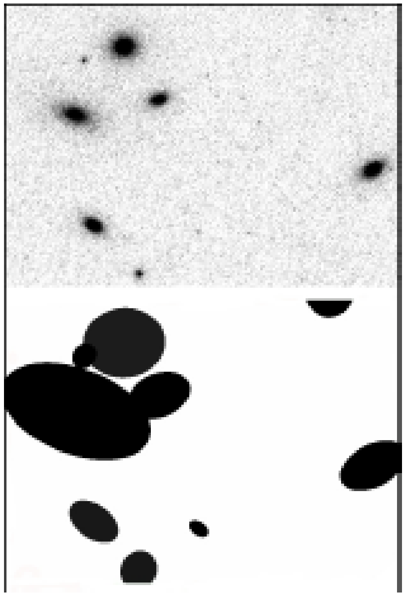

DGCG: Algorithm

3.- Fit order: Brightest to faintest galaxy. Selects PSF. We used the closest star to the galaxy of interest.

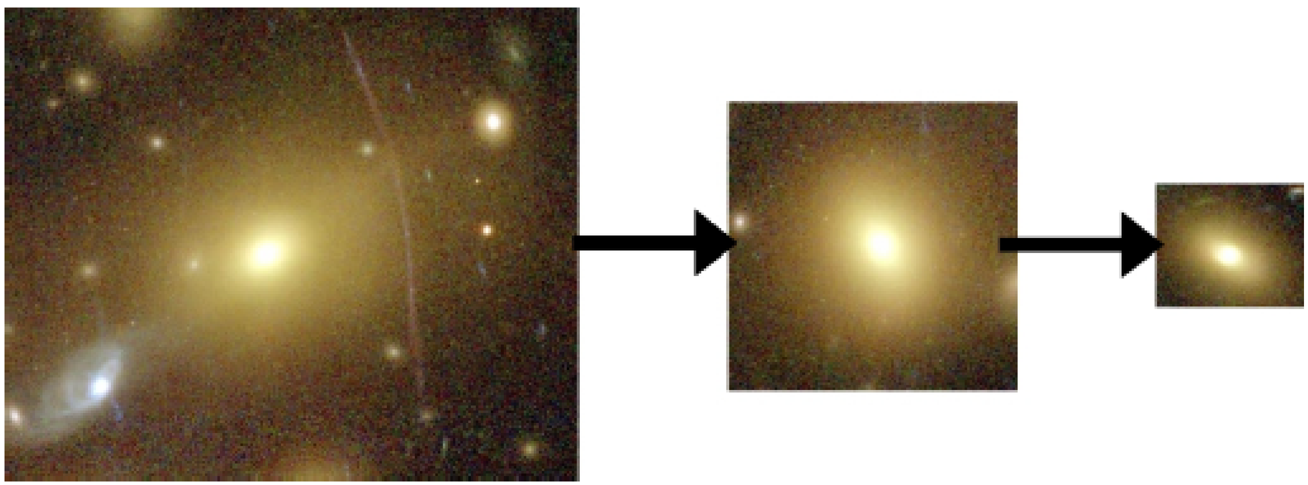

DGCG: Algorithm

4.- Galaxy Fitting:
Simultaneous fitting for Neighbors galaxies. Use Mask for the rest.

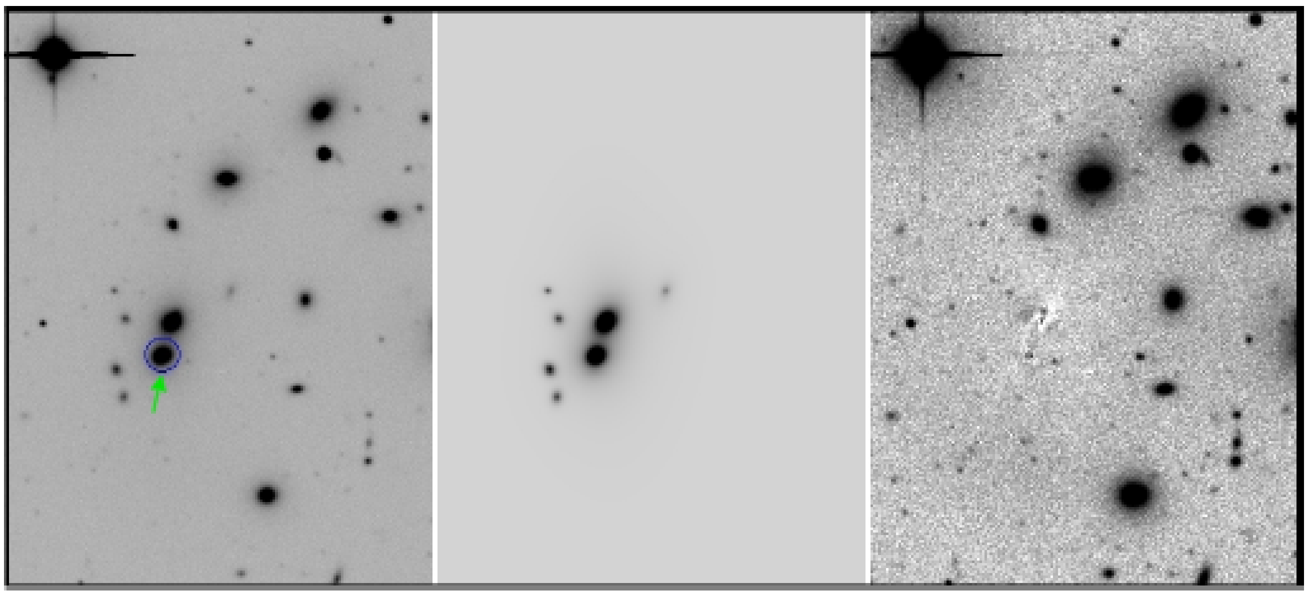

DGCG: Algorithm

5.- Computes Bumpiness, Bulge to Total ratio, SNR, local χ^2_ν within Kron Radius

Bumpiness: Blakeslee et al. (2006)

$$BPN = 10\frac{\sqrt{< [I - S(Re, n)]^2 > - < \sigma_s^2 >}}{< S(Re, n) >} \quad (3)$$

Bars

Surface Brightness Photometry on Artificial Galaxies (Validation)

Fits on GEMS artificial galaxies (SS)

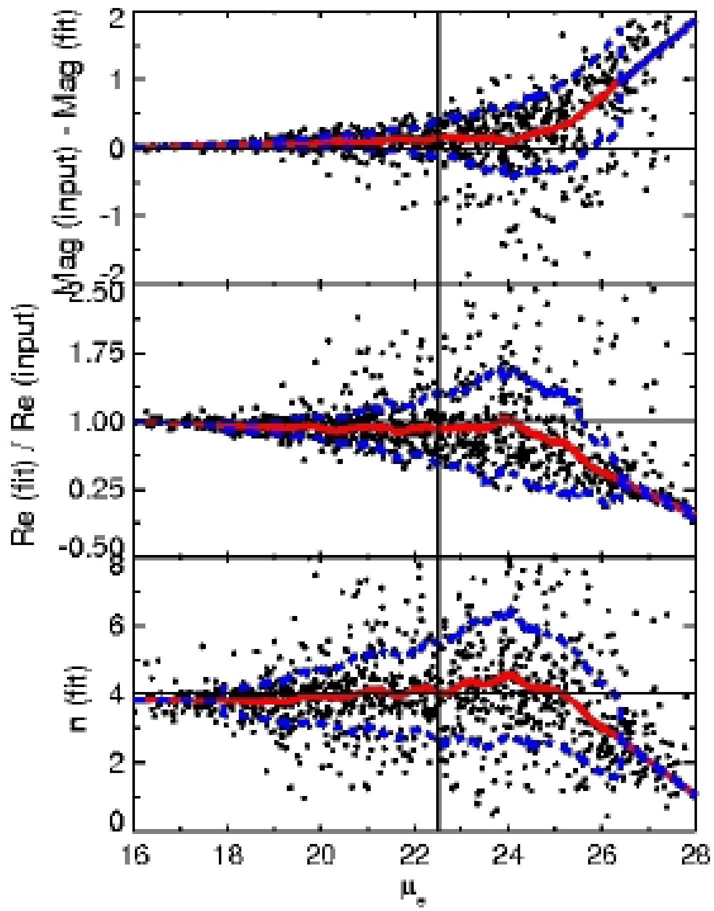

The Sérsic index is hard to recover!

Results

- 1453 from 21 low-z ($0.02 \leq z \leq 0.07$) Abell clusters
- $R = 18$ *mag* completeness limit
- 1453 galaxies with both SS and BD acceptable fits
- The final sample contains 304 E, 557 S0 and 548 S galaxies
- 297 galaxies whose BD fits resulted in Sérsic index less than 0.2 ($n < 0.2$)
- It took 258.89 hrs ($\sim$ 10.79 days) for SS models and 337.23 hrs $\sim$ 15.72 days for the BD models, respectively, to process the whole sample.

Black hole mass correlates with the velocity dispersion of their host spheroidal component.

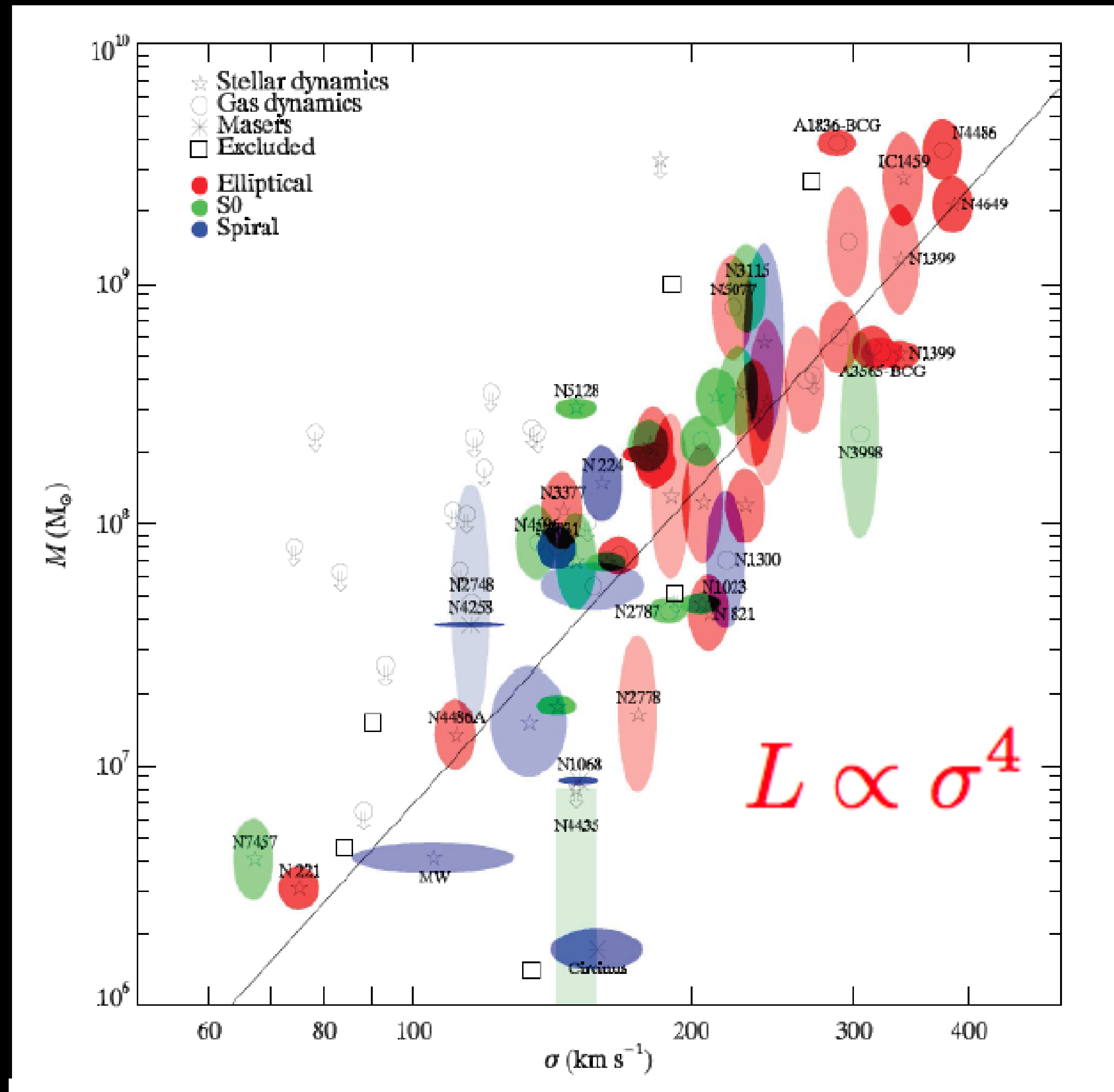

Ultramassive BH : $M_\bullet \geq 10^{10}\ M_\odot$

Distribution of Sérsic Index

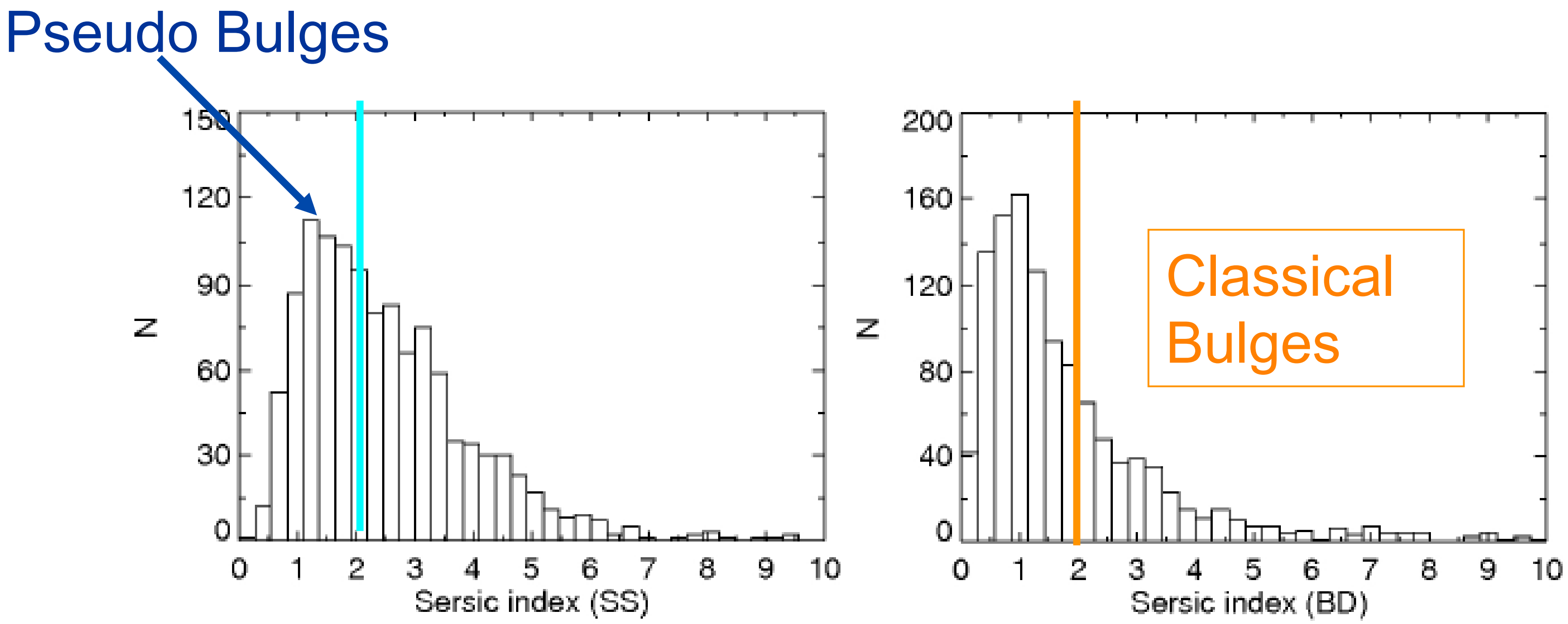

Blanton et al. (2003); Blanton & Moustakas (2009); Fisher & Drory (2010).

Luminosity vs. Sérsic index

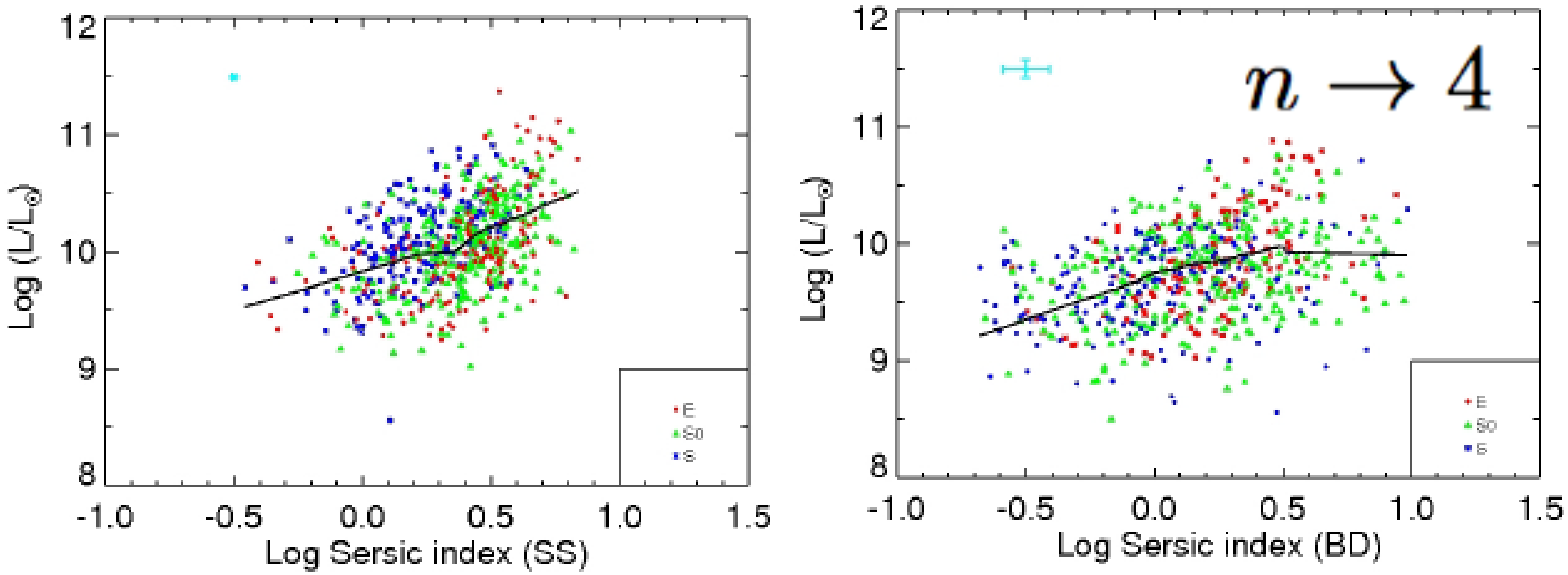

More luminous galaxies have larger Sérsic Indexes (n→4)

Kormendy Relation

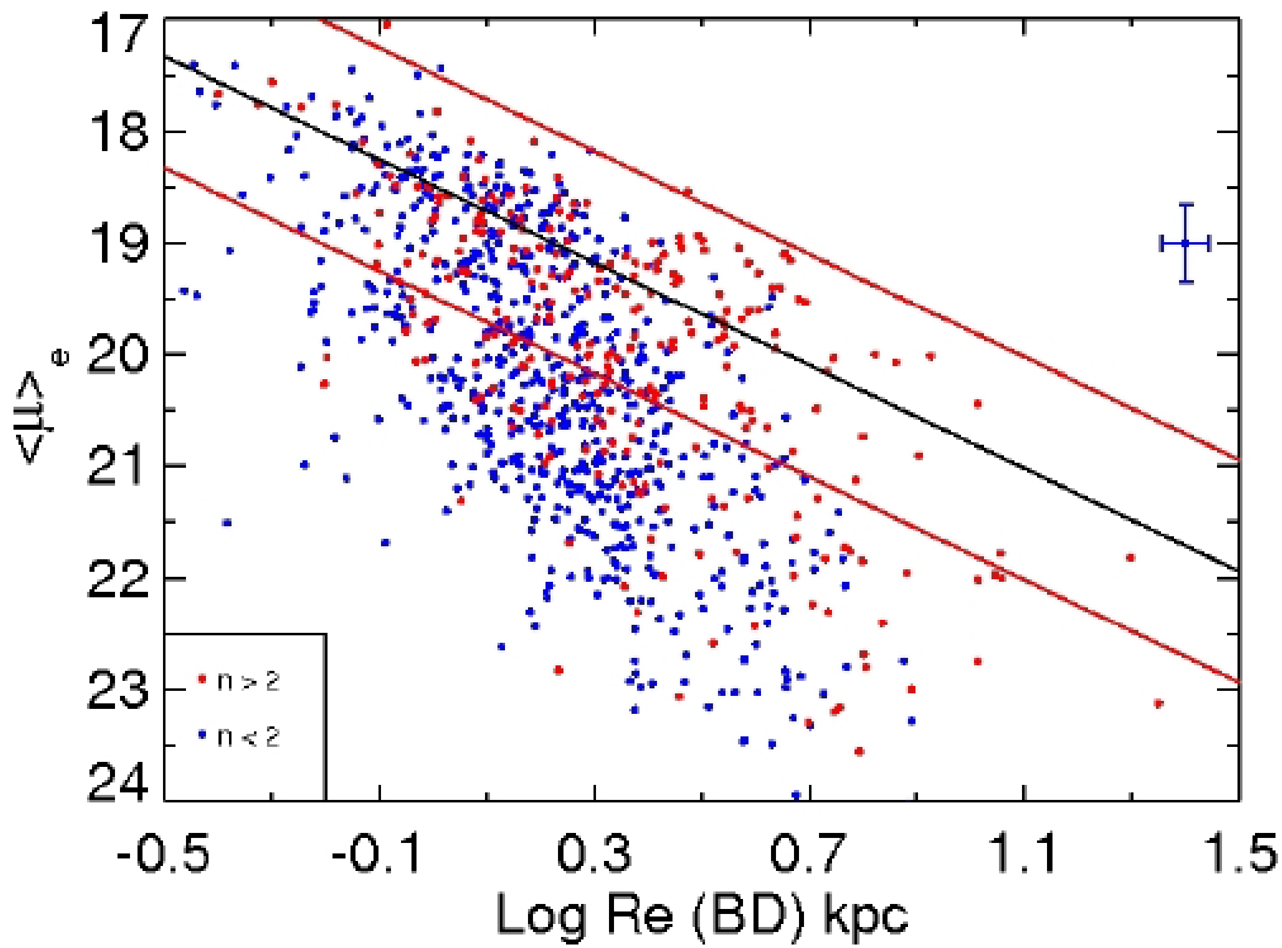

Gadotti (2009)

Pseudobulges: 65% $n < 2$
Diagnostic Diagrams

Luminosity-Size Relation

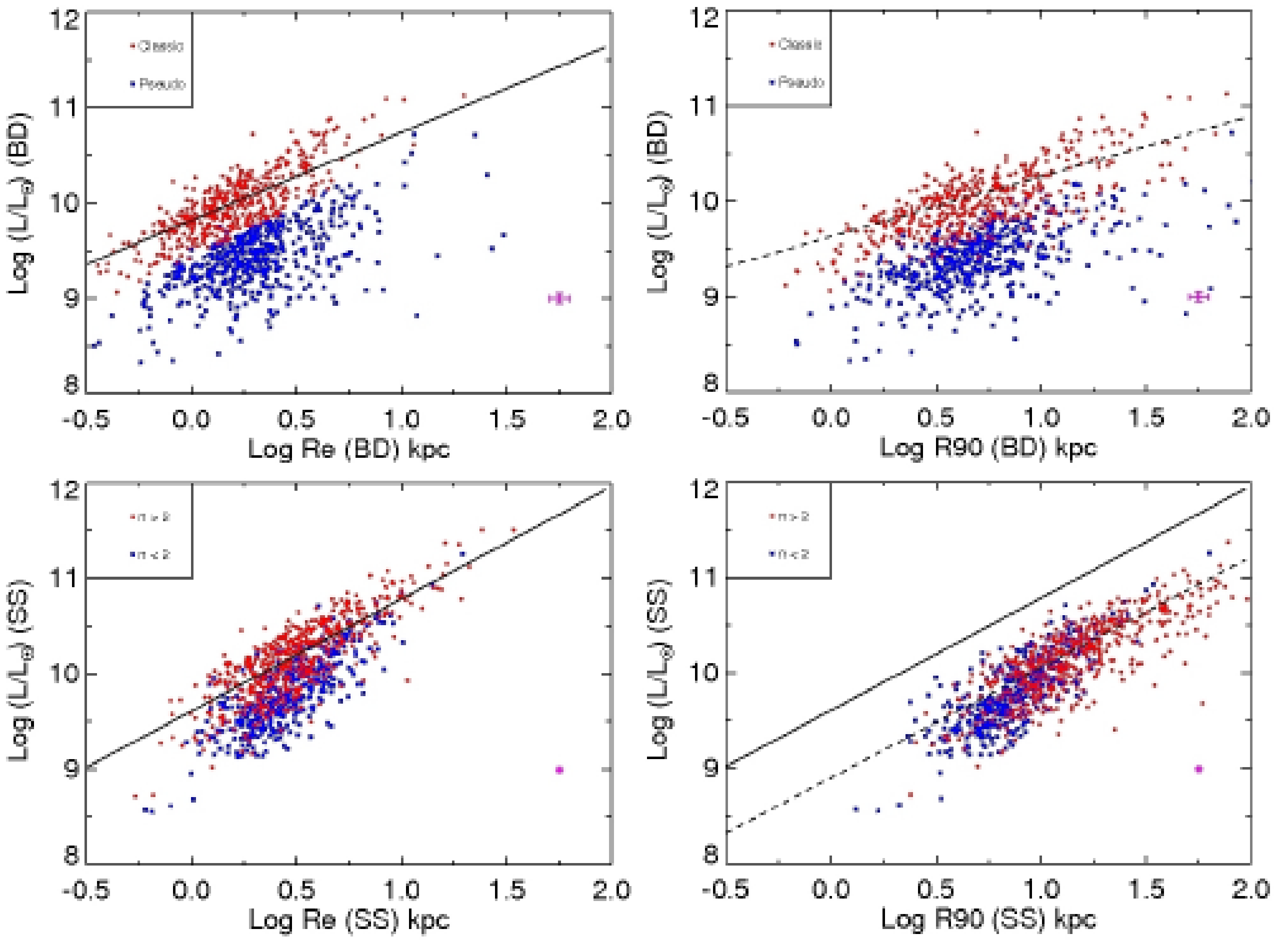

Top: Bulges, Bottom: Galaxy

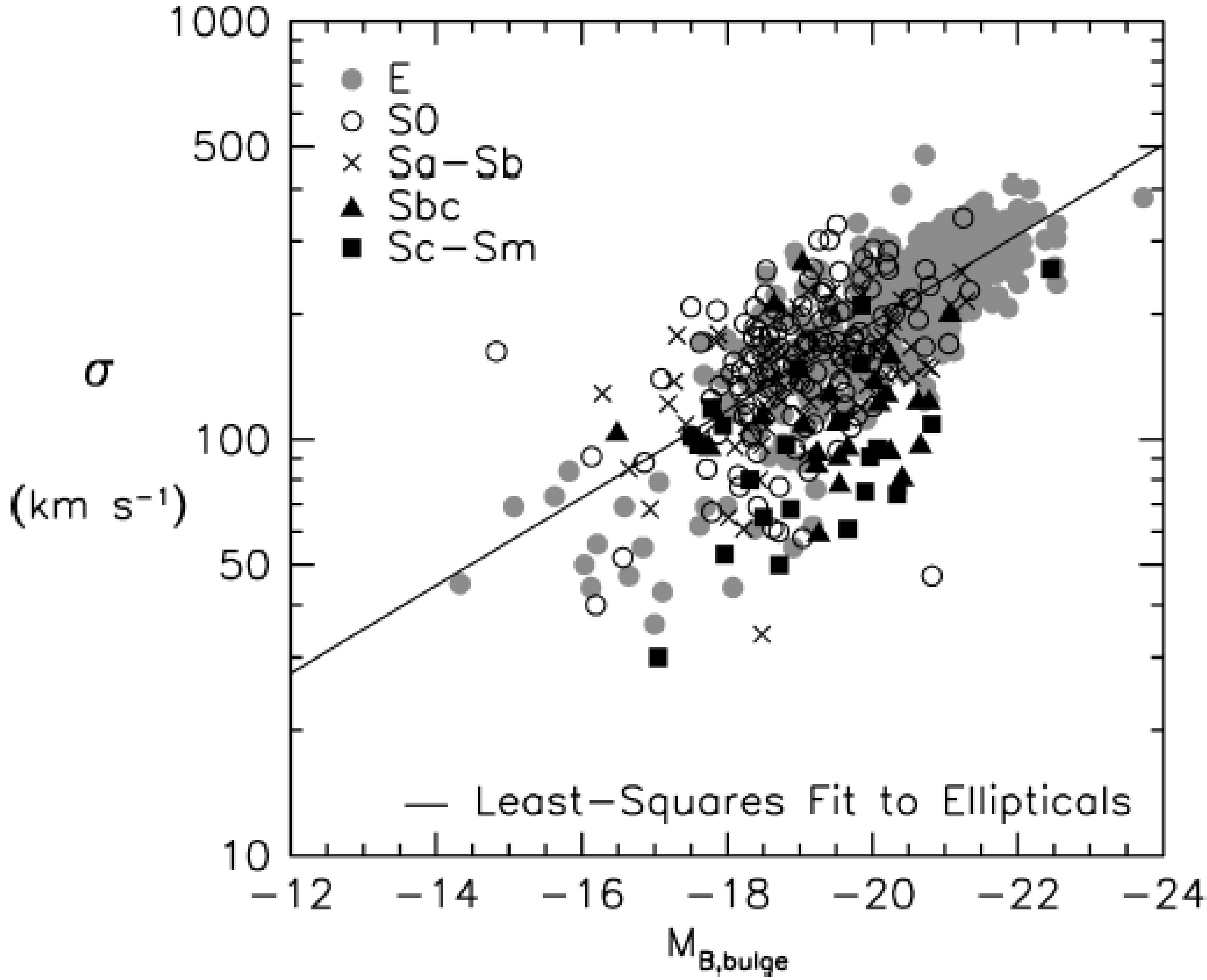

Kormendy & Kennicutt (2004)

Faber-Jackson Relation

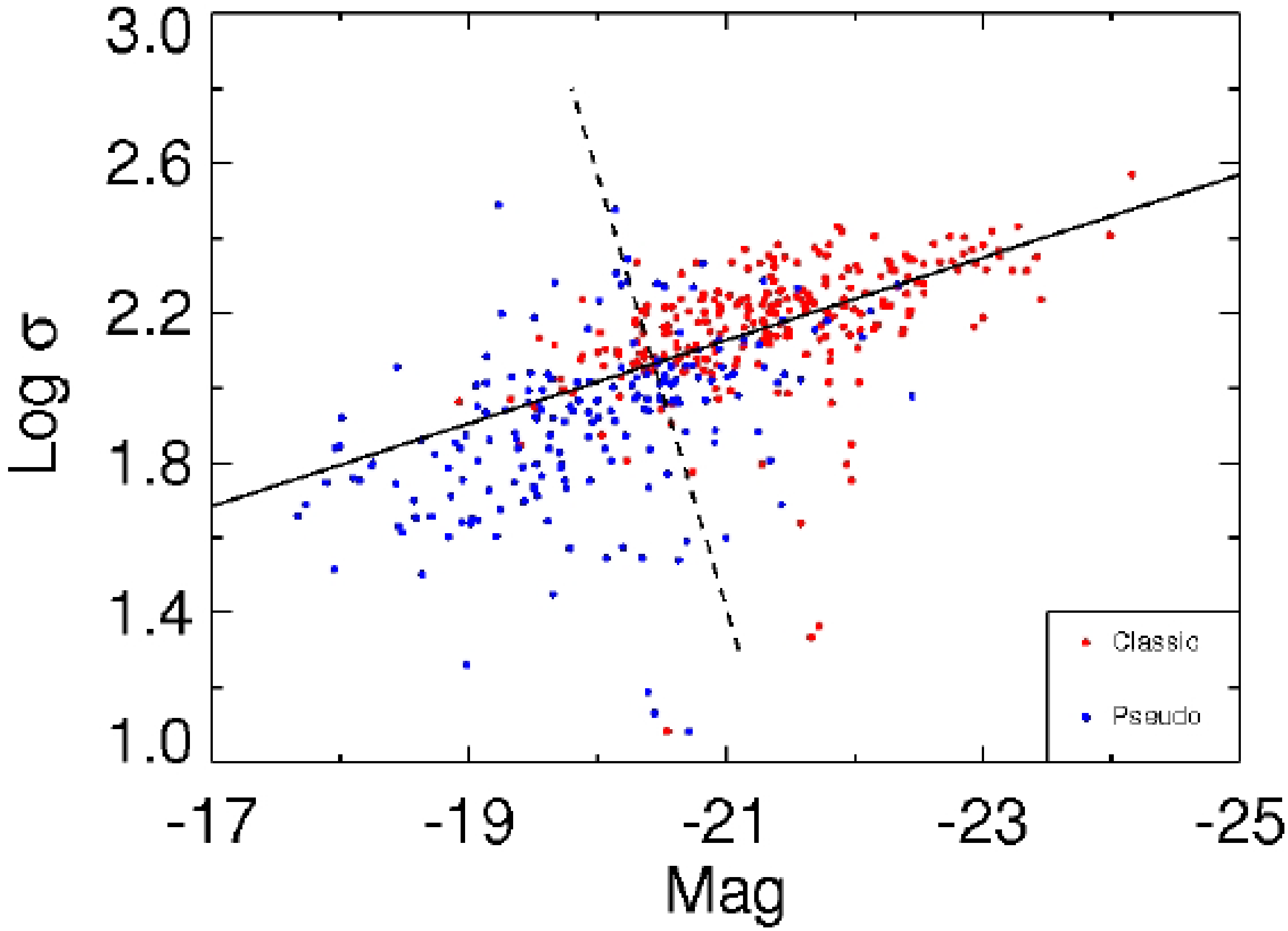

$$\log \sigma = -0.11\ Mag - 0.23, \qquad (8)$$

Fundamental Plane

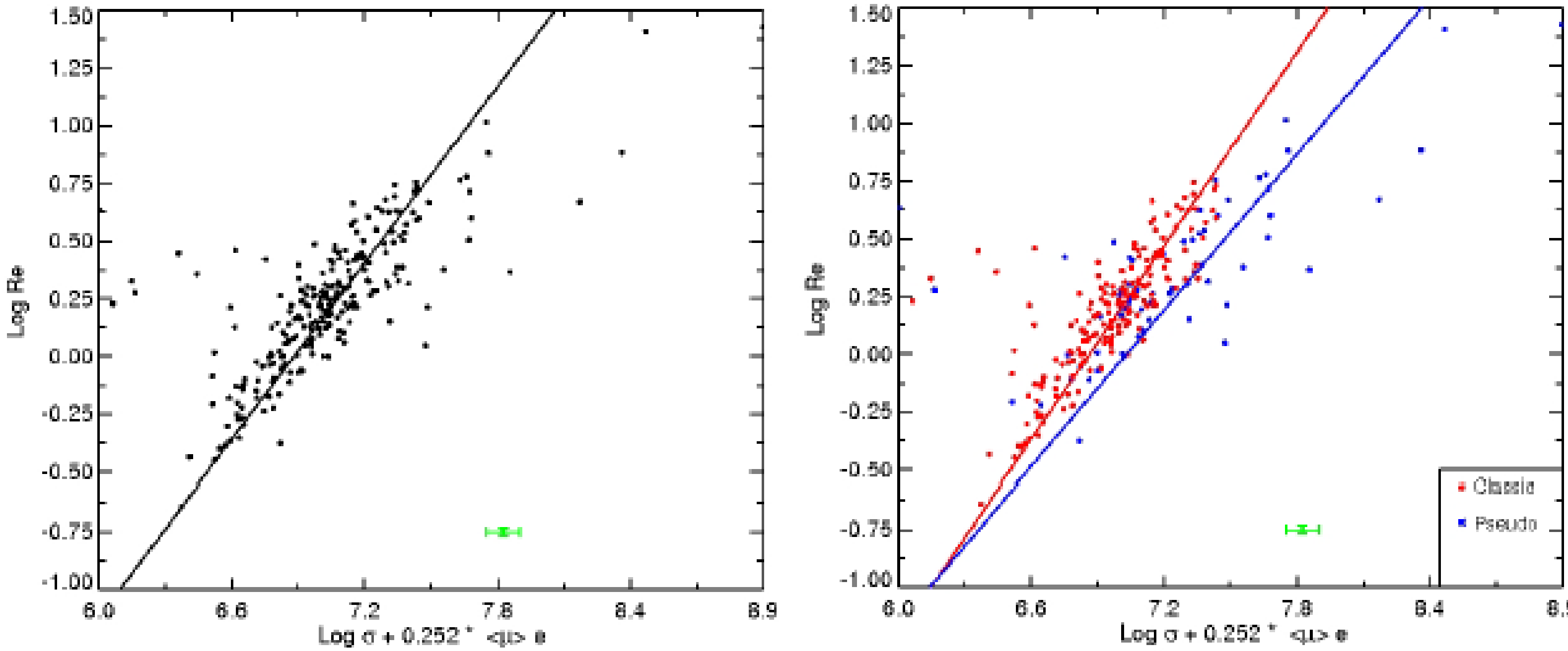

Normal bulges $\log Re = 1.43 \pm 0.023(\log\sigma + 0.252) < \mu >_e + 9.8 \pm 0.16$,

Pseudobulges $\log Re = 1.16 \pm 0.039(\log\sigma + 0.252) < \mu >_e + 8.1 \pm 0.077$

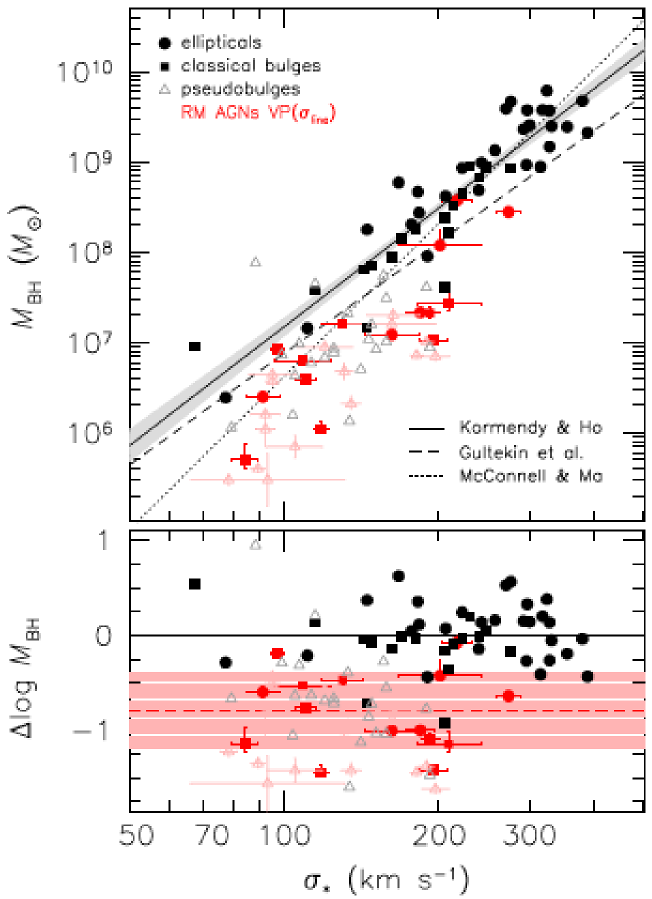

FIG. 2.— (*Top*) The $M_{BH}-\sigma_*$ relation for inactive galaxies (black points) and RM AGNs (red points). The masses for the RM AGNs represent the virial product, $VP = c\tau\Delta V^2/G \equiv M_{BH}/f$, with $\Delta V = \sigma_{line}(H\beta)$ measured from rms spectra. Classical bulges and ellipticals are highlighted as filled symbols, and pseudobulges are plotted as open symbols. Error bars are suppressed for the inactive galaxies to reduce crowding. The best-fit relation of Kormendy & Ho for classical bulges and ellipticals (Equation 2) is given by the solid line; the gray shading represents its 1σ scatter. The fits of Gültekin et al. (2009) and McConnell & Ma (2013) are shown as dashed and dotted lines, respectively. (*Bottom*) Residuals of the data points with respect to the Kormendy & Ho fit for ellipticals and classical bulges. The red dashed line and associated shaded pink band mark the average offset and standard deviation for the 15 RM AGNs hosted by ellipticals and classical bulges: $\langle \Delta \log M_{BH} \rangle = -0.79 \pm 0.42$.

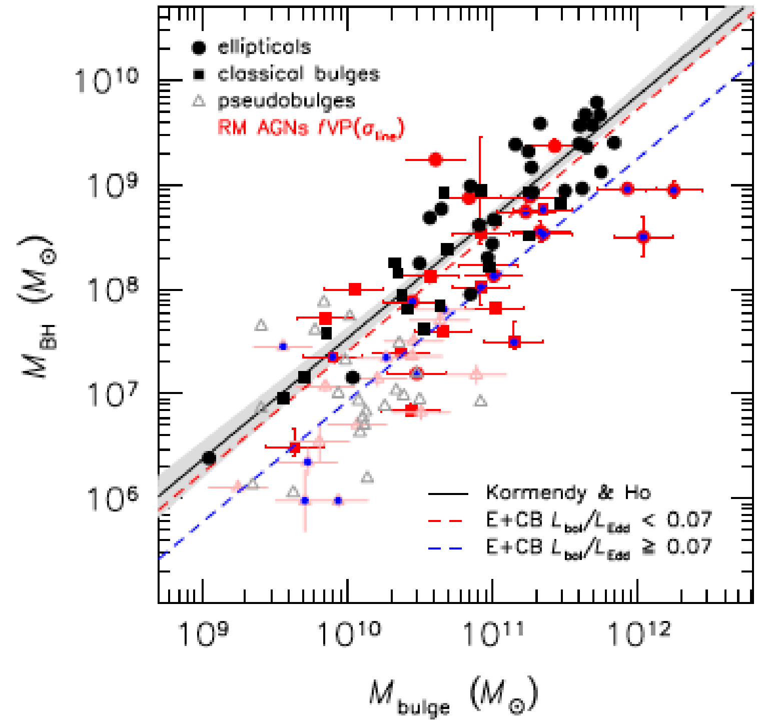

FIG. 5.— $M_{BH}-M_{bulge}$ relation for inactive galaxies (black points) and RM AGNs (red points). Error bars are suppressed for the inactive galaxies to reduce crowding. The virial products, derived from $\sigma_{line}(H\beta)$ measured from rms spectra, have been scaled by $f = 6.3$ for classical bulges and ellipticals and by $f = 3.2$ for pseudobulges. The best-fit relation of Kormendy & Ho for classical bulges and ellipticals (Equation 3) is given by the solid line; the gray shading denotes its 1σ scatter. AGNs hosted by classical bulges and ellipticals with $L_{bol}/L_{Edd} < 0.07$ are denoted by filled red symbols and the red dashed line; those with $L_{bol}/L_{Edd} \geq 0.07$ are highlighted with a blue center and the blue dotted line.

Ho & Kim (2014) bulge mass best correlates BH mass.

What are cD Galaxies?

- cD are supergiant galaxies up to 4 mags. Brighter than M*. They can concentrate up to half the total cluster light.

$$L_{cD} = 5 \times 10^{12}\ L_{\odot}$$

- They are usually found at the center of the galaxy distribution or in local density maxima (Beers & Tonry 1986).
- In some cases they have blue cores (McNamara & O'Connell 1989), or multiple nuclei (Morgan & Lesh 1965)
- 1/4 of the most luminous radio galaxies (WAT) are cD. The term was introduced in a study of optical counterparts of luminous radio galaxies (Matthews, Morgan, & Schmidt, 1964)
- Faint extended envelopes (Oemler 1974, Schombert 1988)

Commonly thought as...

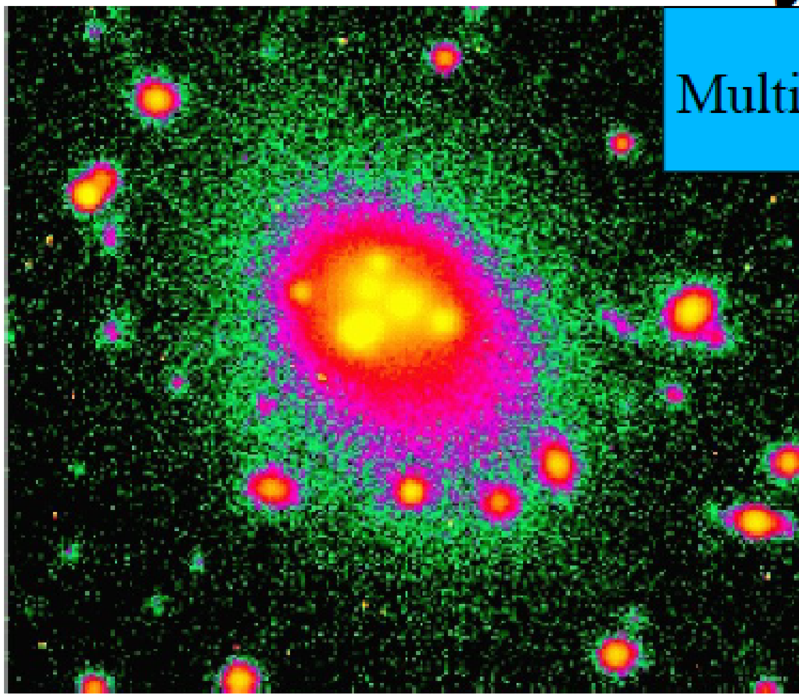

Multiple Nuclei: many of them are just projections

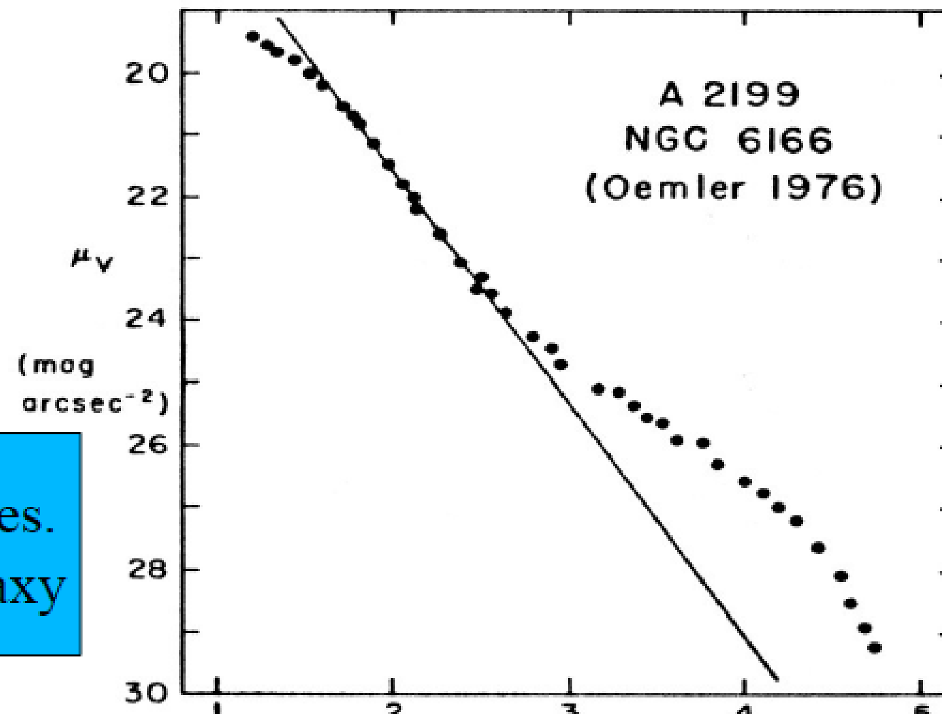

cD galaxies have faint-extended envelopes.
Schombert´s (1988) definition of cD galaxy

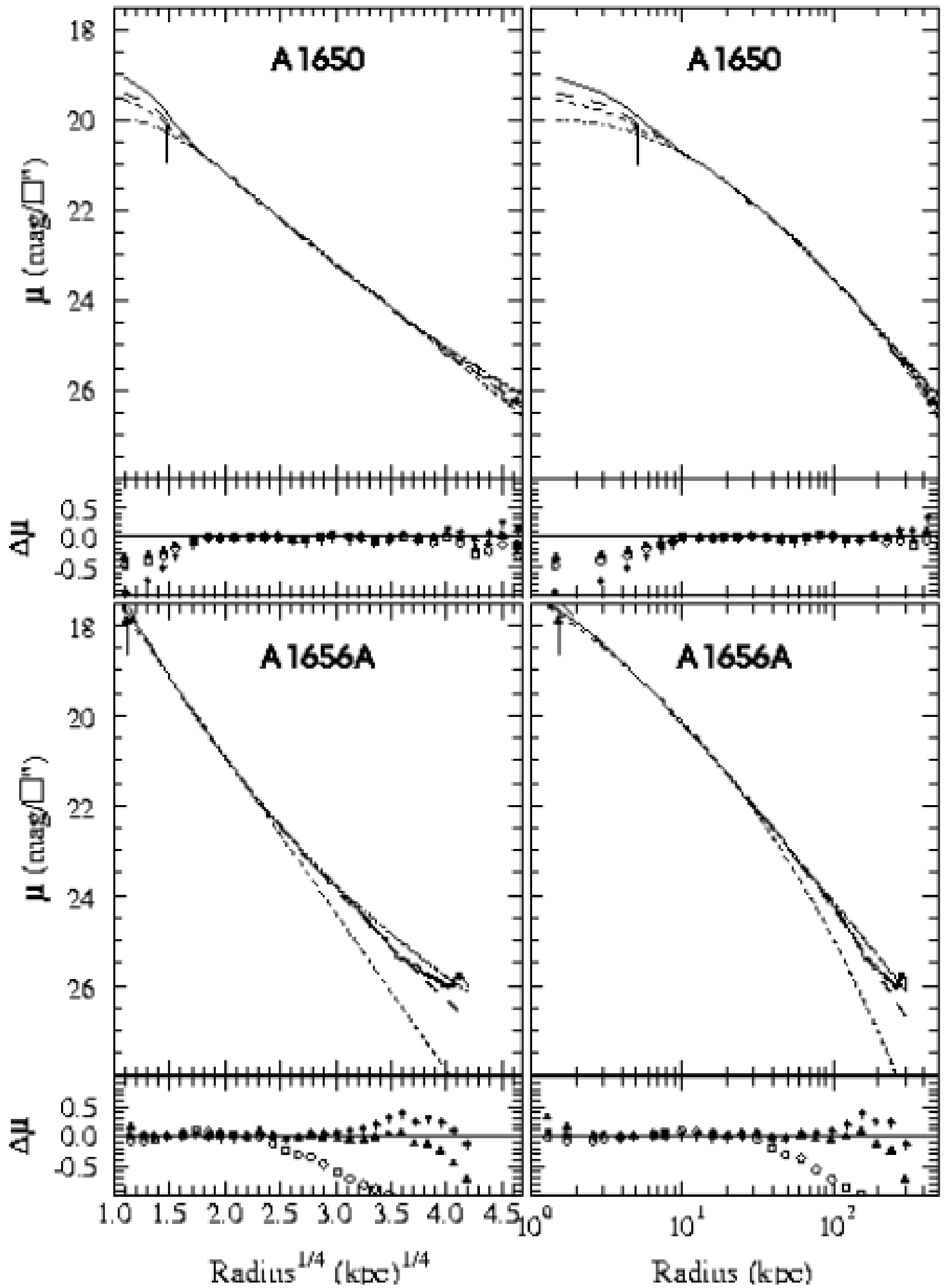

Sometimes
you see the envelopes!!!

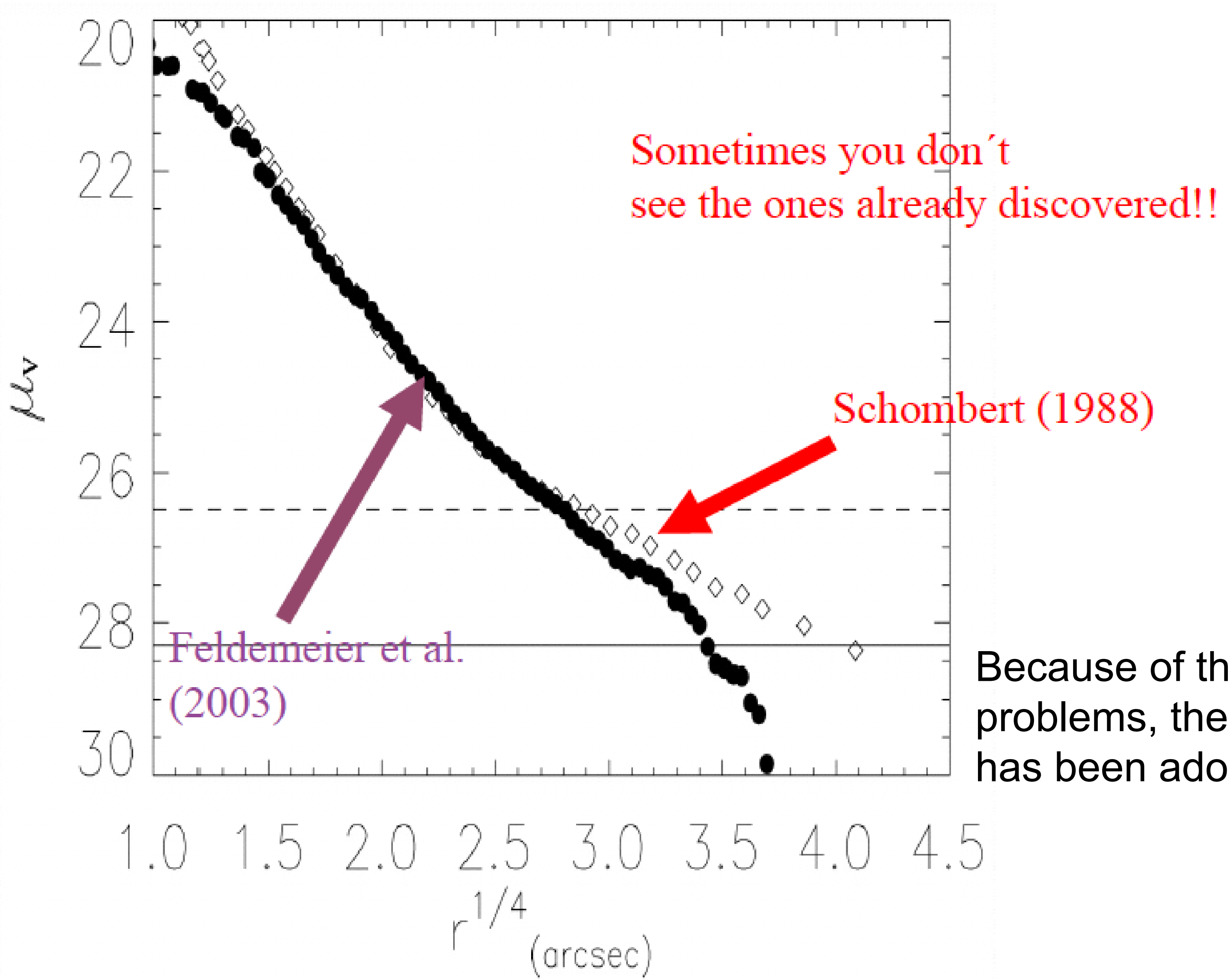

Because of these problems, the term BCG has been adopted.

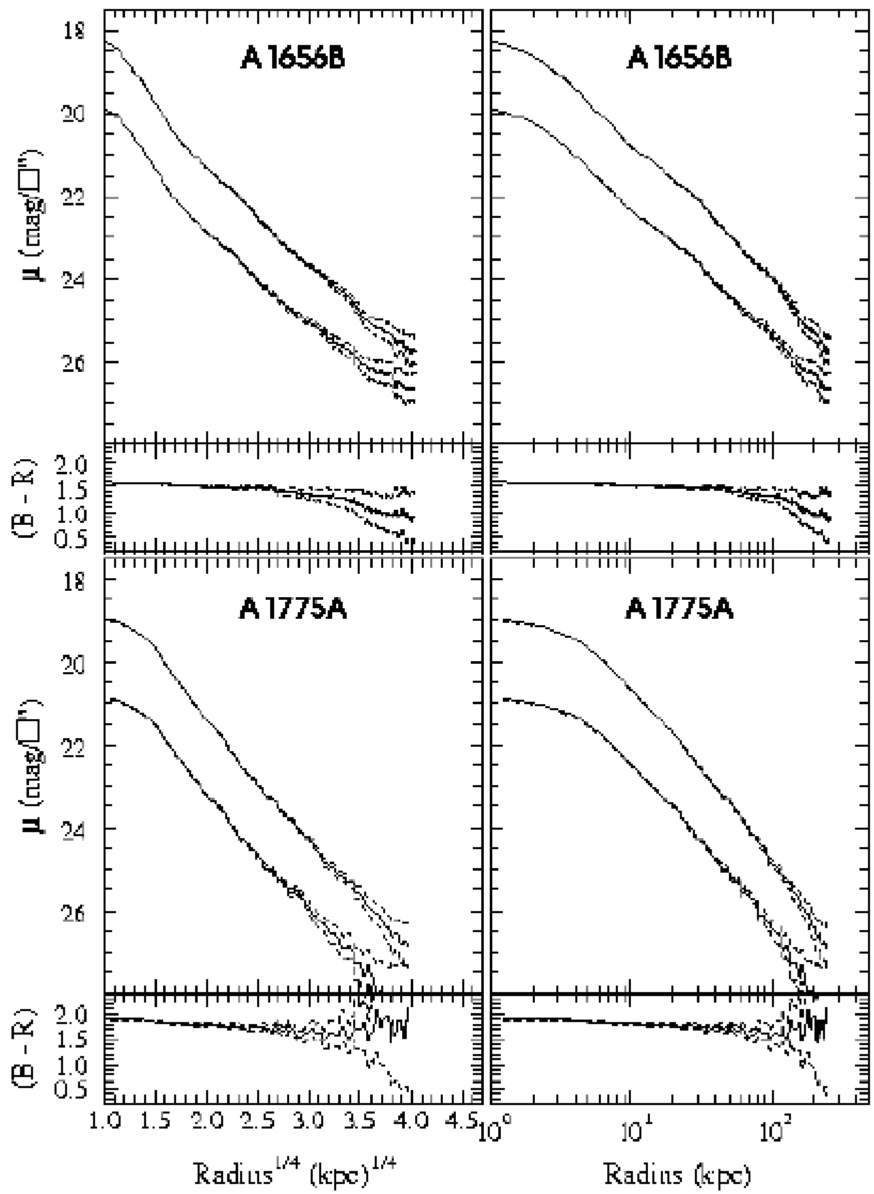

cD galaxies have color gradients, the outkirts are bluer than the inner parts. Beware there are large error... B-R~1.3!!!

The colors of cD envelopes are similar to those of dwarf galaxies

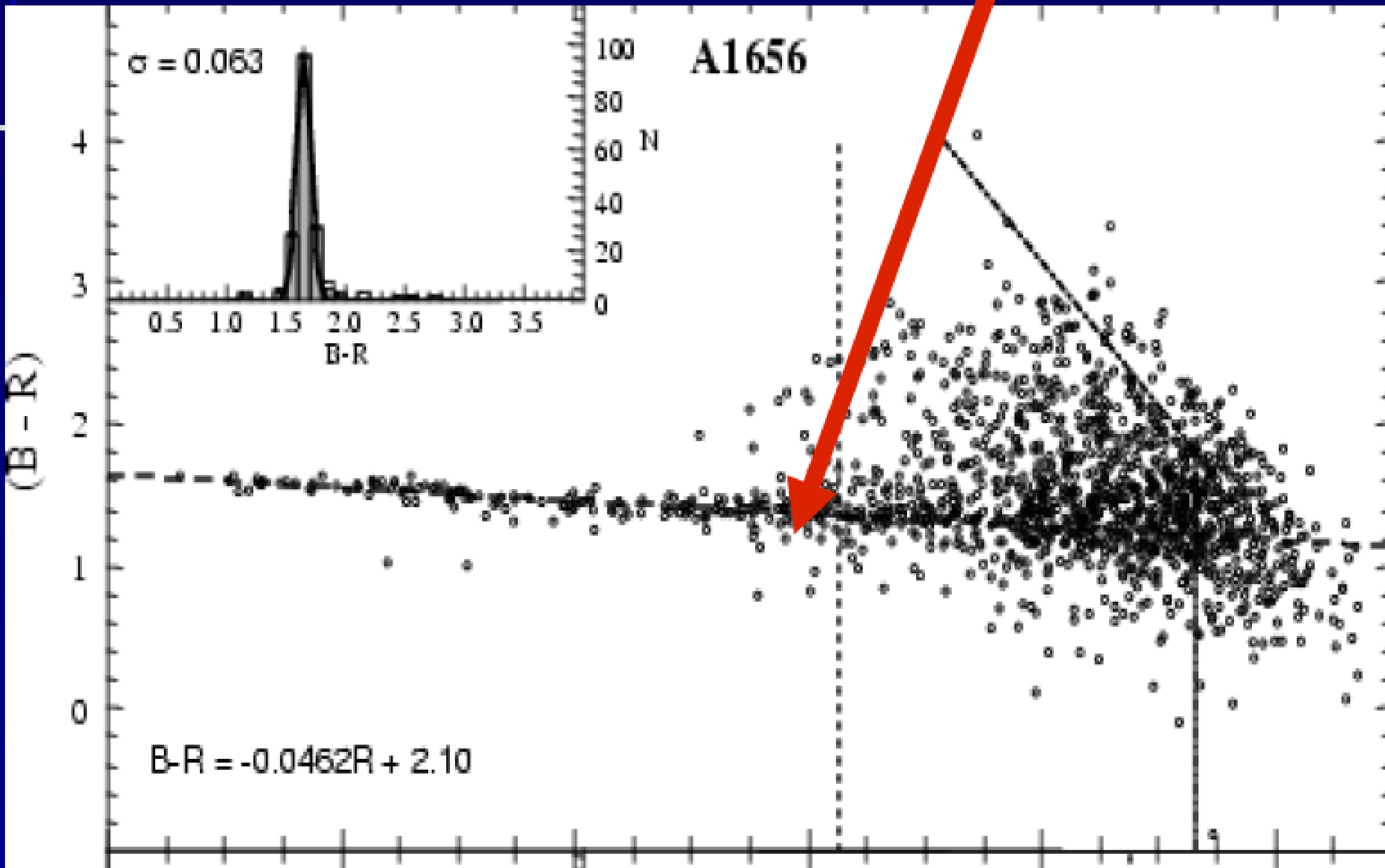

R=14

R=23

How do cD galaxies form?

- Merger of giant galaxies. Not very efficient once the cluster have virialized.
- Dynamical effects: tidal truncation, tidal stripping,♣dynamical friction, etc.
- The fashionable harassment…
- Disruption of Galaxies. We see some evidence at low redshift.

♣Tidal stripping (Aguilar & White 1985,1986)

cD Galaxy Working Definition

- Take Abell statistical sample (1682 clusters). Richness 1 (50 galaxies, m_3 - m_3 + 2 within 1 Abell radius 3 h^{-1}_{50} Mpc) estimated redshift 0.02 < z < 0.2; solid angle approx. 2/3 of the sky (14 438.2 sqr. deg.).
- cD are BGCs in BM I - BM I-II clusters. There are **137 cD galaxies in Abell's sample**. cD galaxies overwhelm satellite galaxies. Classification from Leir & van den Bergh (1977). Leir's M.Sc. Thesis at U of T.

The LF of cD galaxies

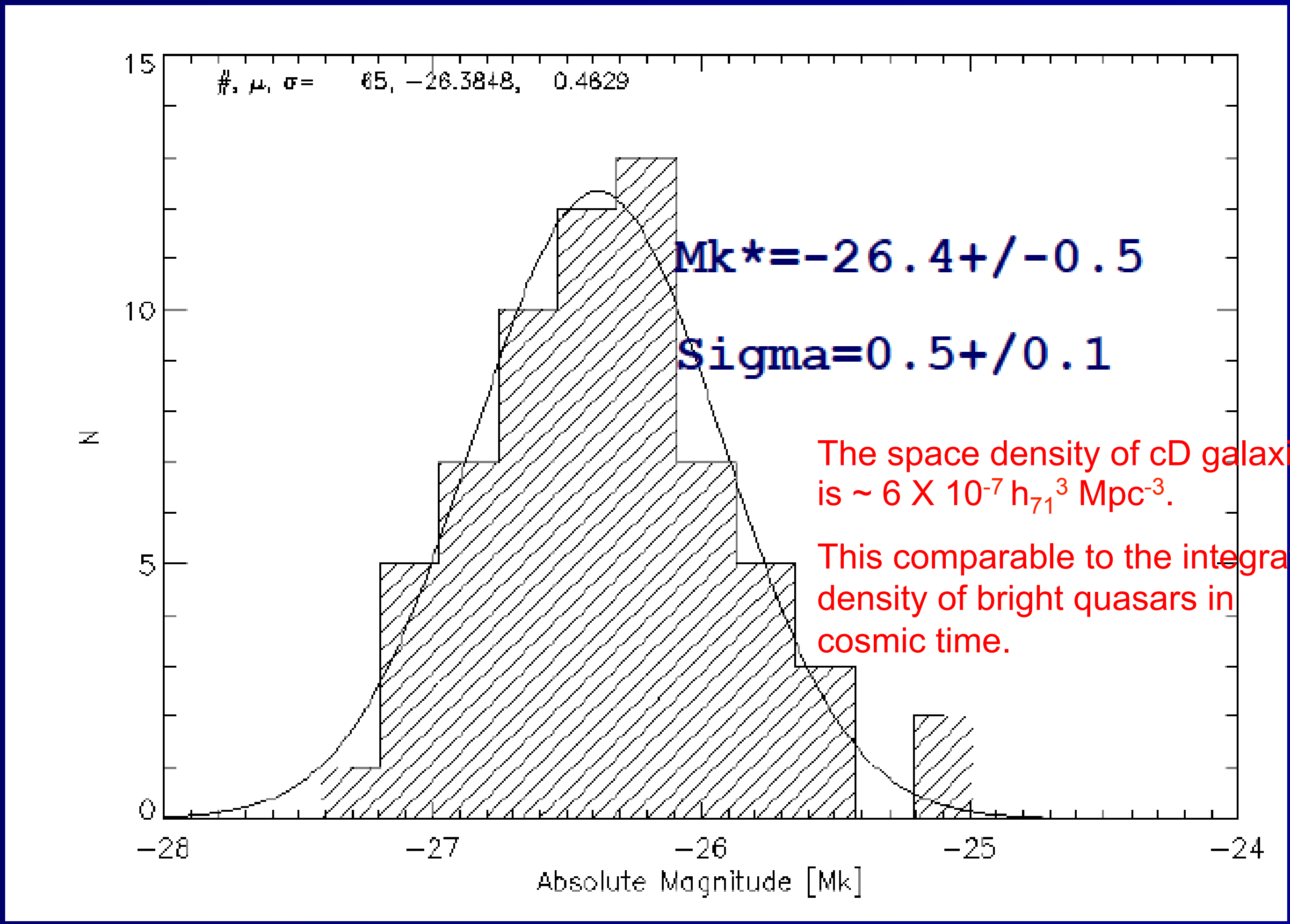

The space density of cD galaxies is ~ 6 X 10^{-7} h_{71}^{3} Mpc^{-3}.

This comparable to the integrated density of bright quasars in cosmic time.

Bright QSO from SDDS DR3, Richards et al. 2006

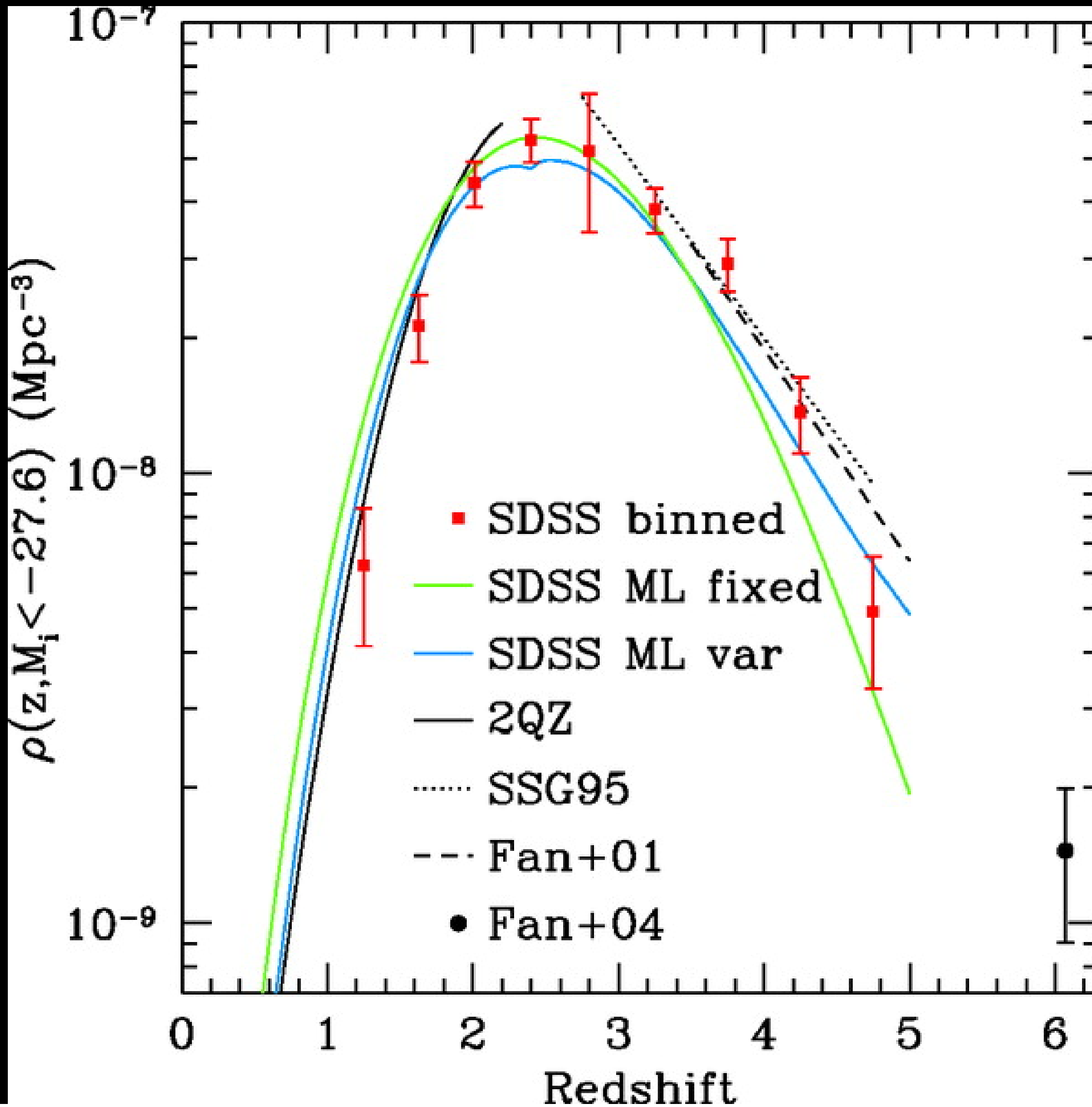

...nection

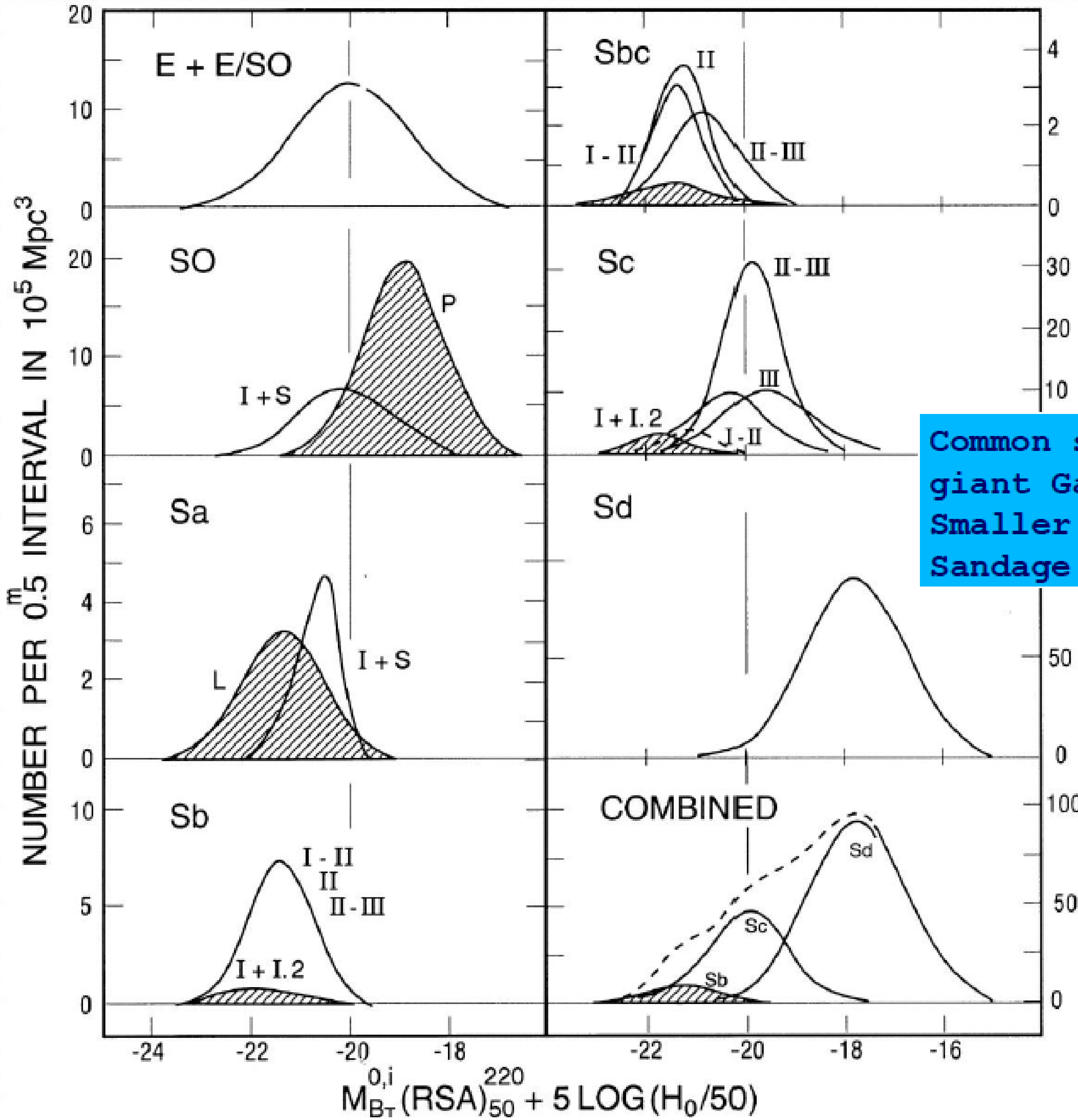

Common shape of F for
giant Galaxies, but
Smaller dispersion. (Sd,0.8)
Sandage 2005, de Lapperent 03

cD Galaxies & Other High Surface Brightness Galaxies follow Gaussian LF, but cDs have the narrowest distribution.

…And we bumped into Postman et al. 2012

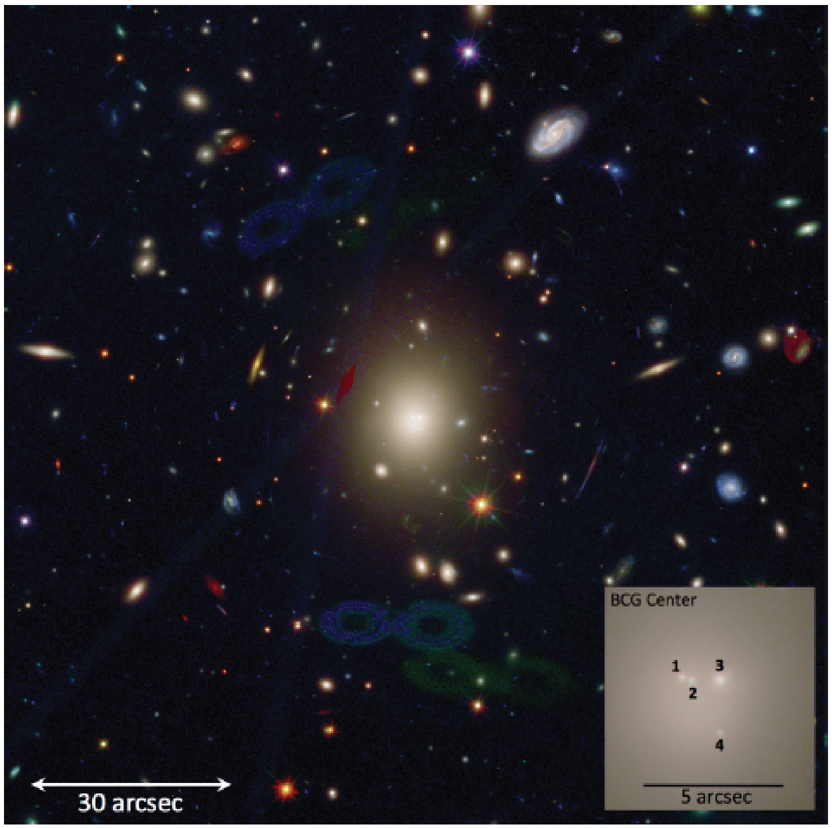

Figure 1. Color composite HST image, from CLASH ACS/WFC and WFC3/IR images, showing the BCG in A2261 and its neighbors in the central 2 × 2 arcminute region of the cluster. The insert in the lower right hand corner shows a zoomed in region centered on the BCG with contrast adjusted to highlight the bright knots (labelled 1,2,3,4) in the core. The orientation is north up and west to the right. The faint "figure 8" patterns at the 6 o'clock and 11 o'clock positions are due to internal reflections in the ACS camera of light from a nearby bright star. The red "diamond" at the 10 o'clock position near the BCG is caused by a gap in areal coverage due to the multiple orientations used in the CLASH survey. The red "blob" at the right edge of the image is a WFC3/IR detector artifact that does not easily calibrate out.

A2261-BGC

z=0.2233

α_{2000}=17:22:27.18

δ_{2000}=+32:07:57.1

$$M_{2500} = (2.9 \pm 0.5) \times 10^{14}\ M_{\odot}$$

Postman et al. 2012 were introducing the largest core yet detected in any galaxy…

details

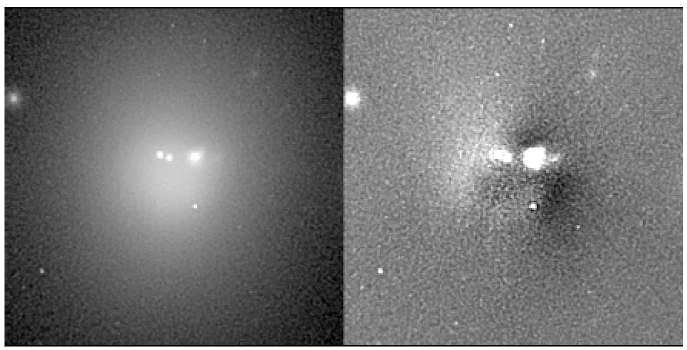

Figure 3. The left panel shows the center of the F814W image of the BCG after Lucy (1974)-Richardson (1972) deconvolution. The region shown is $12'' \times 12''$; (43.2×43.2 kpc) the intensity scale is logarithmic. North is at the top and east to the left. The right panel shows the residuals after subtraction of a model reconstructed from the surface photometry of the BCG. The over all structure of the residuals is a dipole pattern of positive residuals NE of the core and negative residuals to the SW. This suggests that the core is slightly displaced from the surrounding envelope in the SW direction.

The Core o

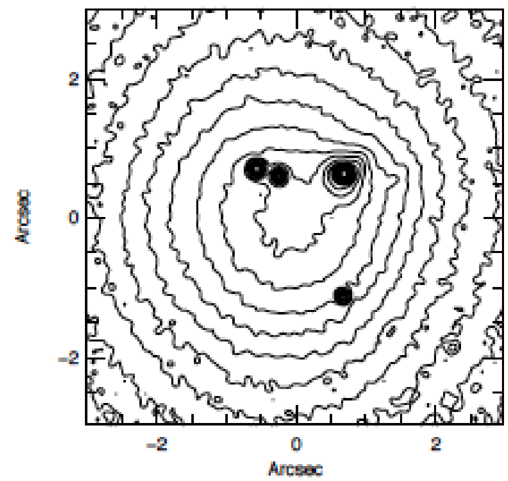

Figure 4. A contour plot of the core of A2261-BCG. The contour levels have an arbitrary zeropoint, but are spaced by 0.25 mag in surface brightness. North is to the top and east to the left. Note that the contour levels are closer together in the SW direction outside the core than they are in the NE, supporting the dipole-like residual pattern seen in Figure 3 and the conclusion that the core is displaced to the SW relative to the envelope center.

The Nuker Law (Lauer et al. 1995)

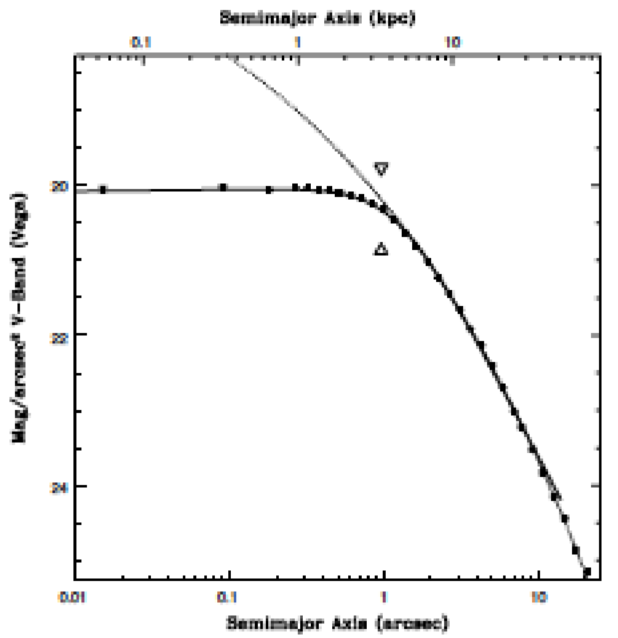

Figure 5. The central surface brightness profile of A2261-BCG as measured (solid points) is shown with two "Nuker-law" profile fits (Lauer et al. 1995). The error bars are smaller than the points, but for the central few measurements. For comparison to previous studies the profile is normalized to $z = 0$ V-band (Vega). The solid line is the best-fitting Nuker-law and features a slightly depressed ($\gamma = -0.01$) cusp as $r \to 0$. The dotted line is an is an $r^{1/4}$-law (an $n = 4$ Sérsic-law) fitted to the envelope. The triangles indicate the cusp-radius.

$$I(r) = 2^{(\beta-\gamma)/\alpha} I_b \left(\frac{r_b}{r}\right)^{\gamma} \left[1 + \frac{r}{r_b}\right]^{(\gamma-\beta)/\alpha}$$

$$r_\gamma \equiv r_b \left(\frac{1/2 - \gamma}{\beta - 1/2}\right)^{1/\alpha}$$

$$\gamma = -0.01, \ \beta = 1.56, \ \alpha = 2.41 \pm 0.18, \ r_b = 1.2''$$

$$r_\gamma = 0''.89 \pm 0''.02; \ 3.2 \pm 0.1\mathrm{kpc}$$

Luminosity vs. Cusp Radius

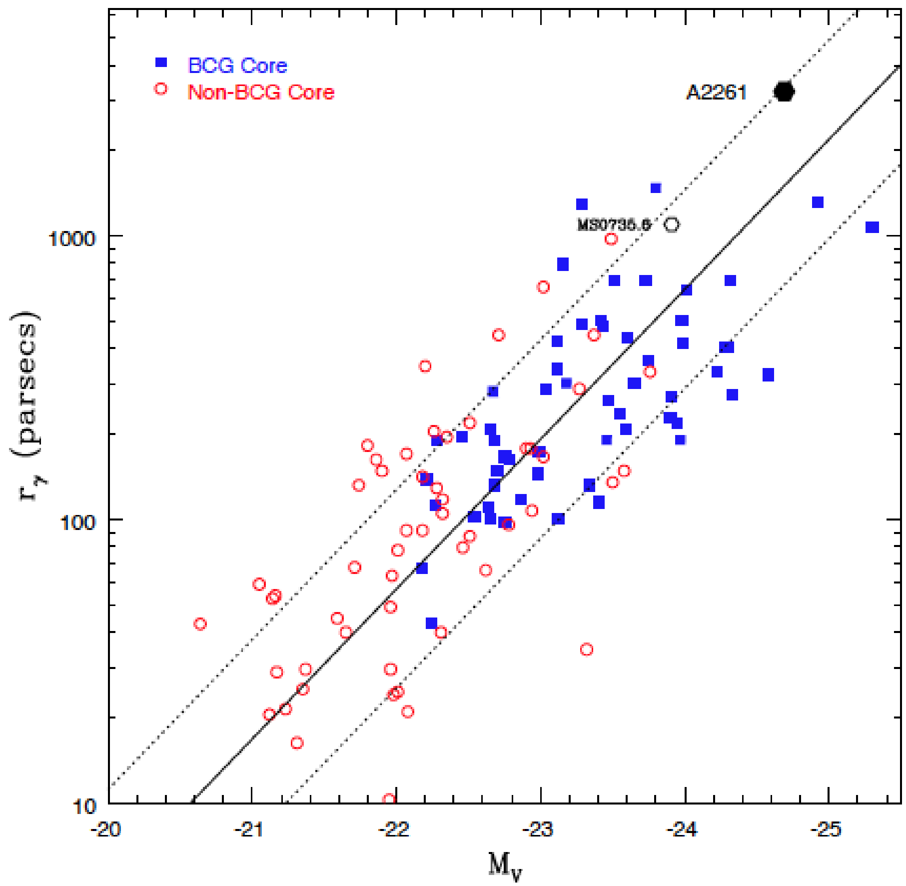

Figure 7. The relationship between cusp-radius and total galaxy luminosity (V-band Vega-based). The galaxy sample plotted was assembled in Lauer et al. (2007a) from a variety of sources (the figure is adopted from Figure 5 in that paper). The BCGs in particular come from the Laine et al. (2002) sample. The Lauer et al. (2007a) $r_\gamma - L$ relationship (also given in equation 4) is plotted; the dotted lines indicate $\pm 1\sigma$ scatter about the mean relationship. A2261-BCG is plotted at the top, clearly has a cusp-radius larger than all other galaxies in the sample. The large core in the MS0735.6+7421 BCG discovered by McNamara et al. (2009) is also plotted for comparison.

But, I recalled Abell 85. James P. Brown and I have worked on it back in 1995 at DA&A, UofT

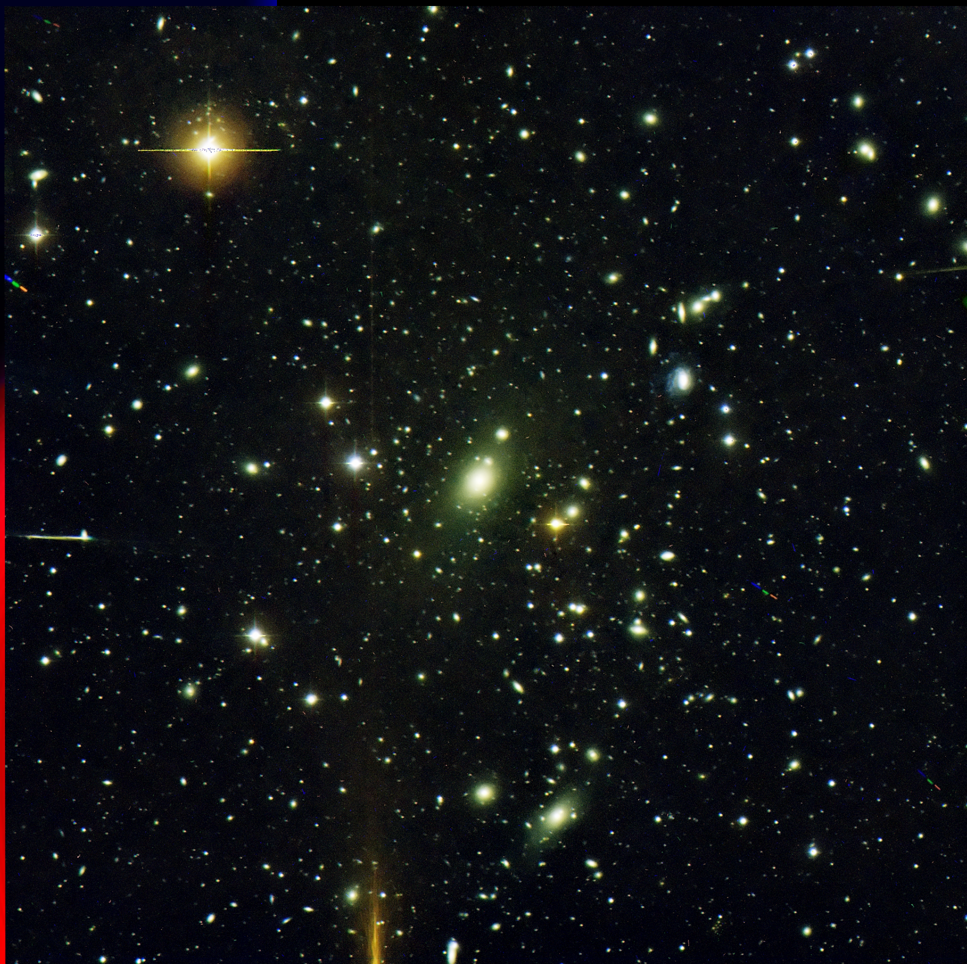

LOCOS, *BRI* images,

Taken with the KPNO 0.9m Telescope using the T2KA CCD. Seeing ~1.6 arcsec

Scale 0.68 arcsec/pixel
z=0.05529 +/- 2.4 X 10^{-4}

Hoessel and collaborators during the early 80's have already singled out that that HOLM 015A had a very large core (modified Hubble Profile)

KPNO 0.9m + T2KA

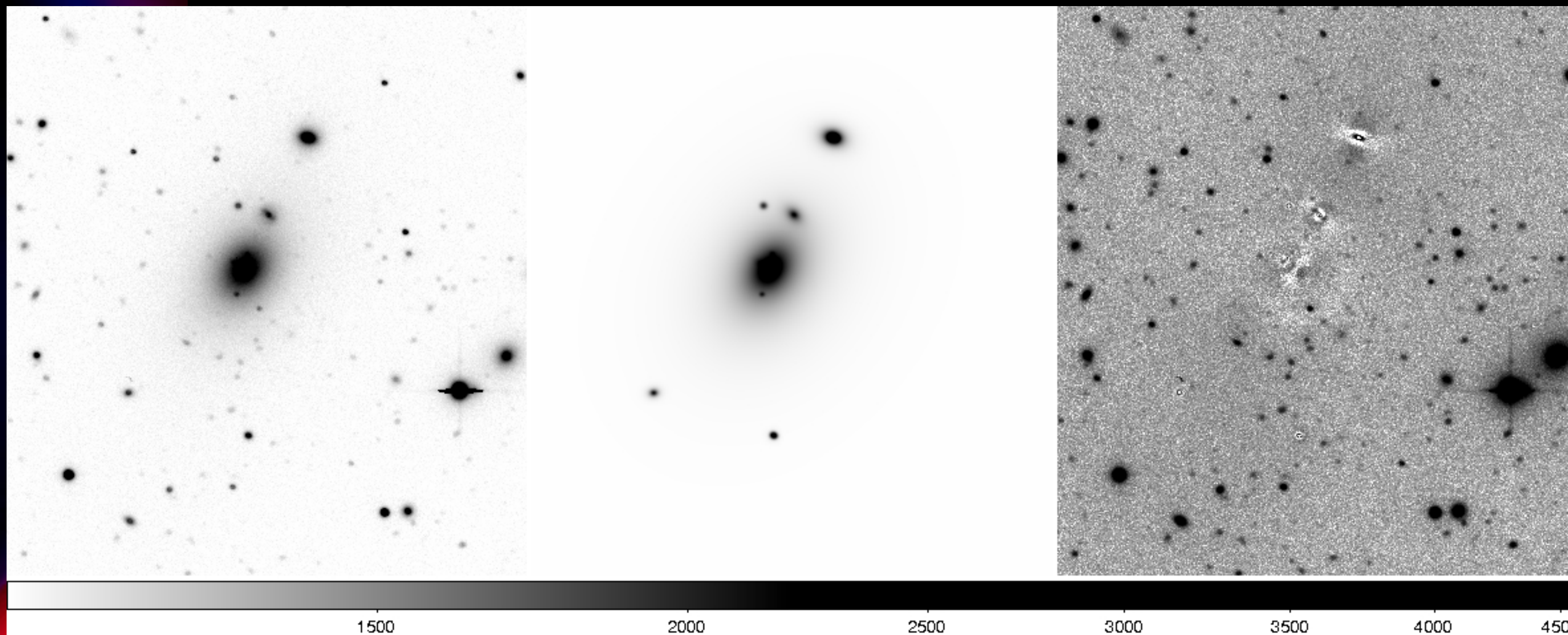

We tried DGCG on A85 using the Nuker Law.

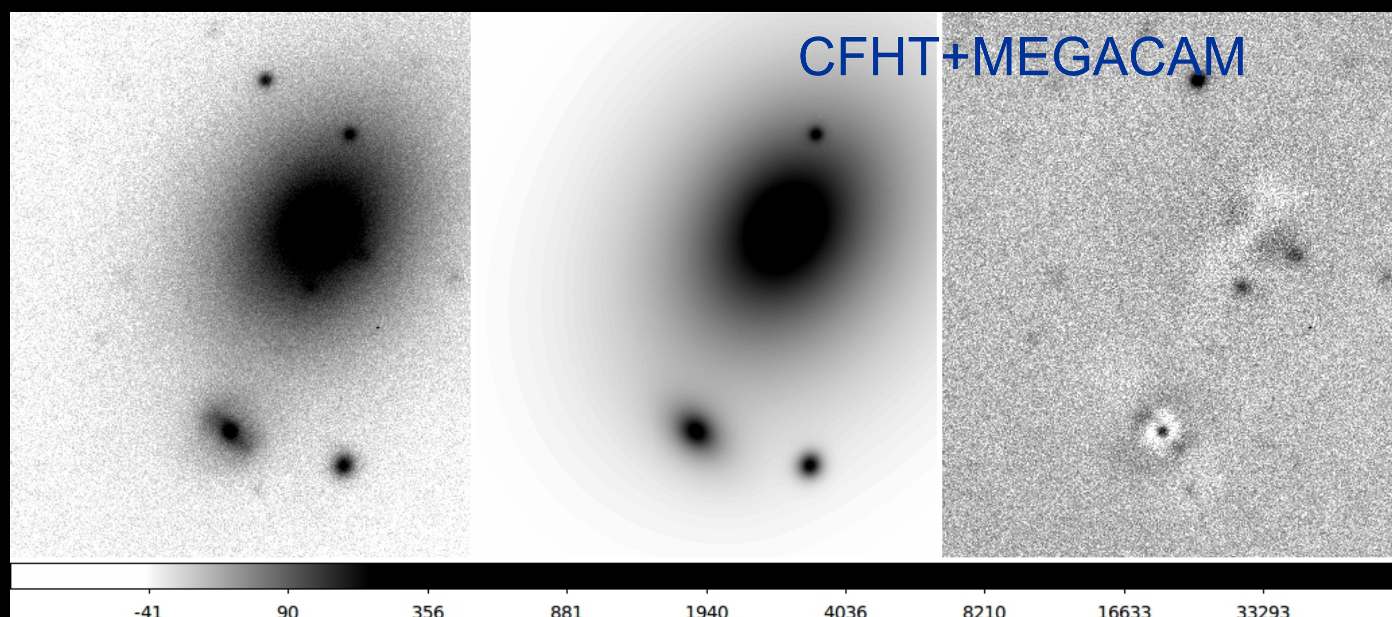

The surface brightness profile of Holm 15A

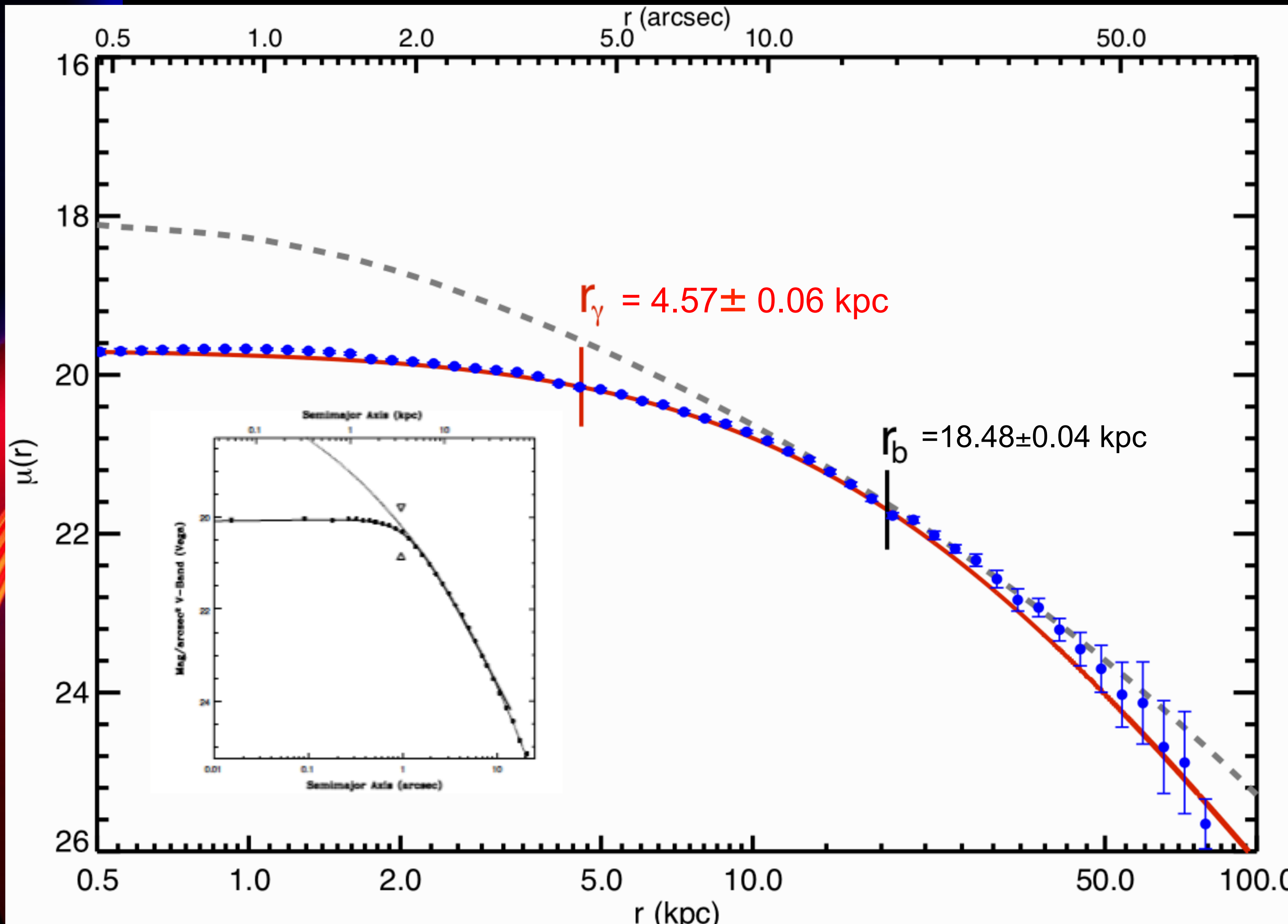

A2266-BGC

$$r_\gamma = 0''.89 \pm 0''.02;\ 3.2 \pm 0.1\mathrm{kpc}$$

Table 1. Holm 15A : Nuker law fits

$\mu_b\ \left[\frac{\mathrm{mag.}}{\mathrm{arcsec}^2}\right]$	r_b [arcsec]	r_b [kpc]	α	β	γ	r_γ[kpc]	e	P. A.	Data
21.78 ± 0.01	17.21 ± 0.04	18.48 ± 0.04	1.24 ± 0.01	3.33 ± 0.02	0.0 ± 0.0	**4.57 ± 0.06**	0.26	-33.33	⋆
22.32	19.09	20.50	1.22	3.62	0.0	**4.57**	0.24	-34.07	•

COLUMNS– 1: surface brightness, 2: break radius in arcsec, 3: break radius in kpc, 4: outer power index, 5: power index at r_b, 6: outer power index, 7: cusp radius in kpc, 8: ellipticity, 9: position angle in degrees,10: Data Source.

⋆ LOCOS (López-Cruz 1997), Telescope: KPNO 0.9m, CCD: T2KA; pixel scale: $0.''68$/pixel. filter: R (Kron-Cousins), exposure time: 900 s, seeing: $1.''6$ FWHM, FOV: $23.'2 \times 23.'2$.

• MENeaCS (Sand et al. 2011), Telescope: CFHT 3.5m, CCD: MegaCam; pixel scale: $0.''187$/pixel, filter: r' (SDSS), exposure time: 120 s, seeing: $0.''74$ FWHM, FOV: $0.^\circ96 \times 0.^\circ94$.

Note. — centroid: $\alpha_{2000} = 00^h41^m50.^s467$, $\delta_{2000} = -09^\circ18'11.''57$

The Largest Core known so far!!!

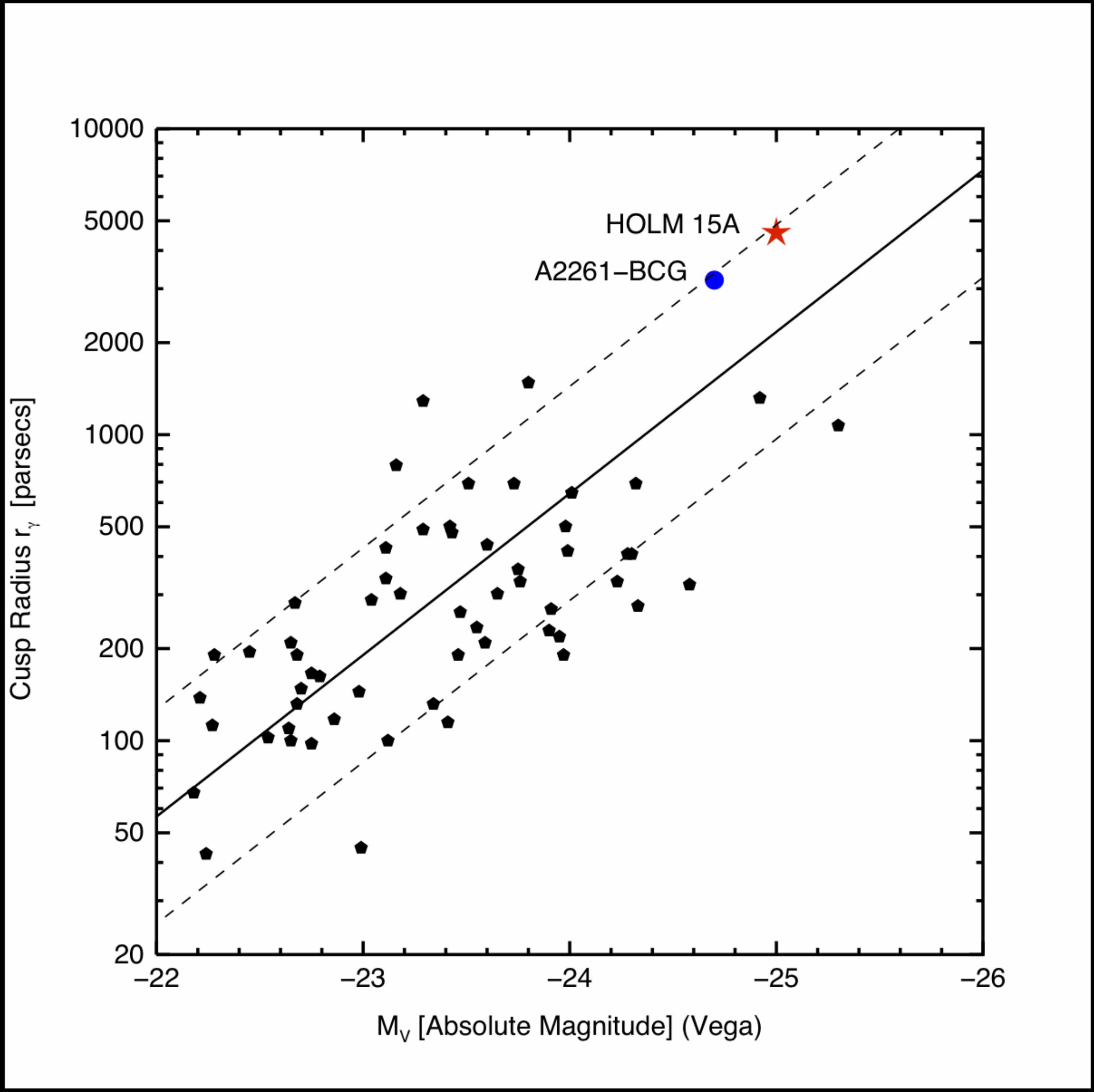

Bonfini et al. (2015) has challenged this result.

THE ASTROPHYSICAL JOURNAL, 807:136 (10pp), 2015 July 10 BONFINI, DULLO, & GRAHAM

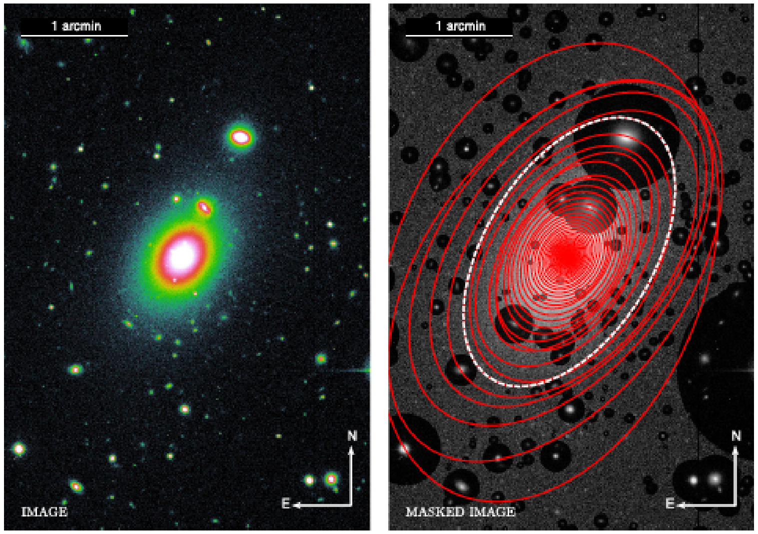

Figure 1. CFHT-MegaPrime *r*-band image (left) and relevant mask (right) for Holm 15A. The masked areas (see Section 2) have been arbitrarily decreased in intensity so as to still show the contaminating objects. We overplot the elliptical isophotes from IRAF.*ellipse* (the boxiness of the ellipses is not considered in this representation). The dashed ellipse corresponds to the limiting surface brightness at which we truncated our 1D analysis ($\mu \sim 25.5$ mag arcsec^{-2}; see Section 2). This ellipse also corresponds to the physical extent of the 2D fit (everything outside the dashed curve was masked for the 2D fit; see Section 2).

Table 1
CFHT-MegaPipe Image Characteristics

Target (1)	R.A. (J2000) (hh:mm:ss) (2)	Decl. (J2000) (dd:mm:ss) (3)	D (Mpc) (4)	$m - M$ (mag) (5)	Camera/Filter (6)	Exposure (s) (7)	Scale ($''$/pixel) (8)
Holm 15A	$00^h41^m50^s.5$	$-09^\circ18'11''$	253	37.02	MegaPrime/r	120	0.186

Notes. Details of the CFHT-MegaPrime image used for the current work. (1) Target name. (2, 3) Target coordinates from NED. (4) Luminosity distance from NED, corresponding to a redshift $z \sim 0.057$ (see footnote 2). (5) Distance modulus. (6) CFHT camera and filter. (7) Total exposure time. (8) Image pixel scale.

Core-Sérsic (Trujillo et al. (2004)

$$I(R) = I' \left[1 + \left(\frac{R_b}{R}\right)^{\alpha}\right]^{\frac{\gamma}{\alpha}} \exp\left(-b\left[\frac{R^{\alpha} + R_b^{\alpha}}{R_e^{\alpha}}\right]\right)^{\frac{1}{(\alpha n)}}$$

$$I' = I_b 2^{-\frac{\gamma}{\alpha}} \exp b \left(\frac{2^{-\frac{\gamma}{\alpha}} R_b}{R_e}\right)^{\frac{1}{n}}$$

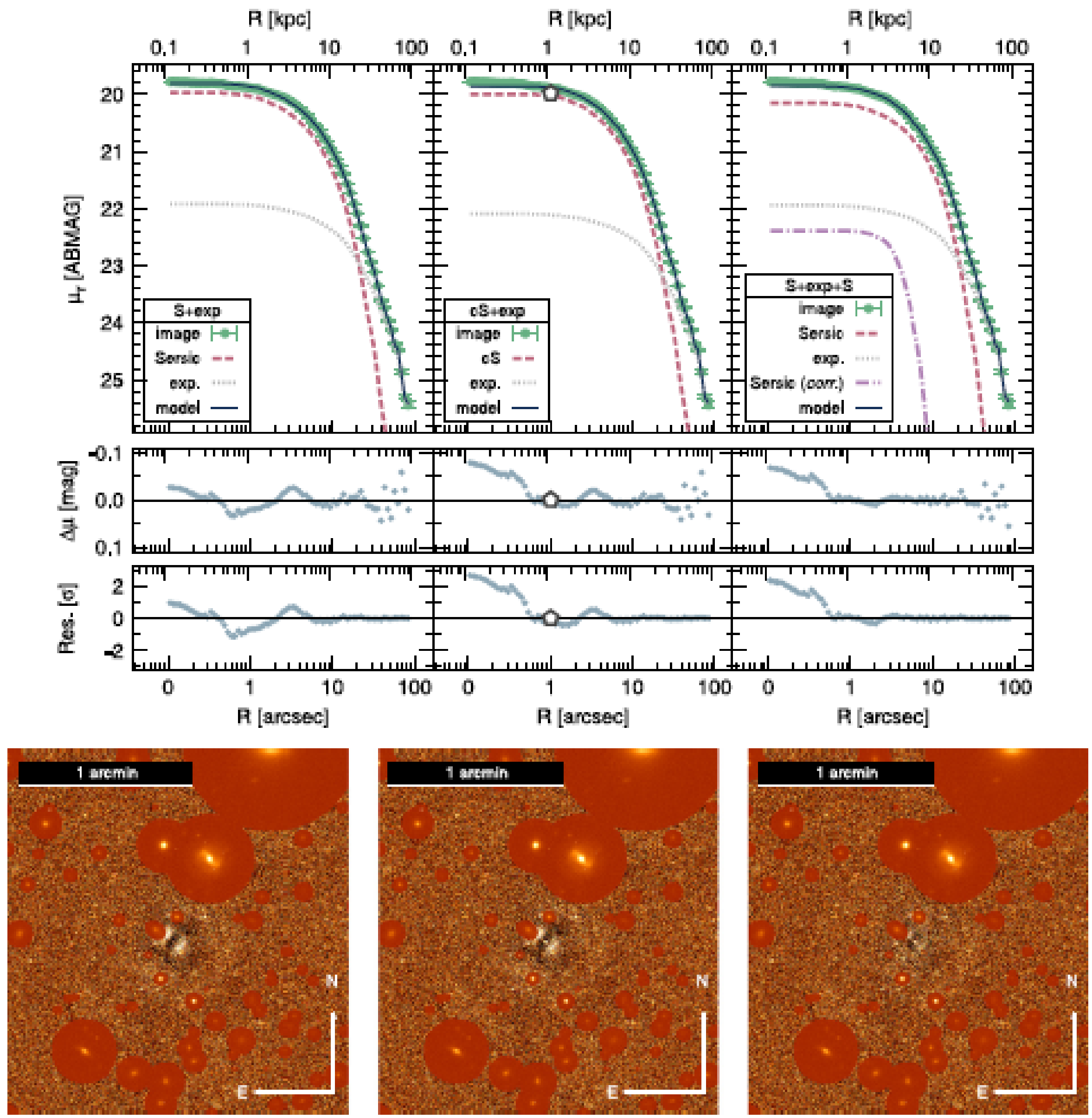

Figure 4. 2D image analysis: results of the fits to the 2D image of Holm 15A performed assuming a Sérsic+exponential model (left); a core-Sérsic +exponential model (middle); and a Sérsic+exponential model plus an additional inner Sérsic component intended to compensate for the single ellipticity of the 2D model components (right). Top. The green data points represent the major-axis surface brightness profile measured over the isophotes defined using IRAF.*ellipse* (i.e., the same measurement presented in Figure 2). The curves represent the surface brightness profile of the model images measured over exactly the same isophotes. The continuous curves show the global models, while the dashed curves represent their sub-components. We stress that these are *not* fits to the 1D profile, but rather surface brightness measurements (projections) of the 2D models. The pentagon indicates the location of the core-Sérsic model's break radius. The panels underneath the profiles represent the data residuals about the fitted models, first expressed in terms of the difference in surface brightness, and then in terms of residuals (in units of counts) divided by the standard deviation as measured on the "sigma" image. Bottom. The actual residual images that were minimized by Galfit-Corsair. Masked objects are highlighted as in Figure 1.

Bonfini et al. (2015) used GALFIT-CORSAIR and showed that Core-Sérsic profile doesn´t work for Holm 15A, but recovered Lópe-Cruz et al. (2014) Nuker fit.

The Mexican Contribution to the field (ca. 1978)!!

THE TEMPERATURE AND DYNAMICS OF THE IONIZED GAS IN THE NUCLEUS OF OUR GALAXY

LUIS F. RODRIGUEZ* AND ERIC J. CHAISSON†
Harvard-Smithsonian Center for Astrophysics

Received 1978 August 18; accepted 1978 September 26

ABSTRACT

Observations of the H65α (23.4 GHz), H84α (10.9 GHz), and H94α (7.8 GHz) radio recombination lines from Sgr A West are presented. We suggest that a core-halo model can satisfactorily account for the reported radio and infrared observations of this source. Due to instrumental limitations, the observed infrared lines are dominated by the core, while the observed radio radiation arises mostly in the halo. Although more than a factor of 10 brighter than the halo, the core is responsible for only about one-fourth of the integrated thermal continuum from Sgr A West. Our model implies that the neon abundance determination from infrared observations, previously considered consistent with the solar value, should be revised upward by a factor of 4. This suggested enrichment of neon relates strongly to our derivation of an unusually low electron temperature, $T_e = 5000 \pm 1000$ K, since nebular cooling is expected to be enhanced by an overabundant heavy-element content. The dynamical structure of Sgr A West can be explained in terms of Keplerian rotation due to the gravitational field of the normal stellar population plus a central mass point of $5 \times 10^6\ M_\odot$.

… a central mass point of $5 \times 10^6\ M_\odot$

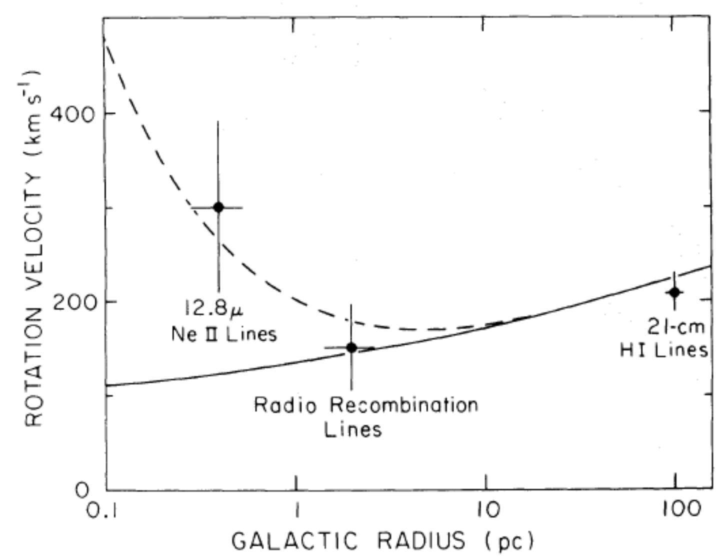

FIG. 4.—A tentative rotation curve for the galactic nucleus. *Solid curve*, model having normal stellar population; *dashed curve*, model having the same normal stellar population plus a mass point of $5 \times 10^6\ M_\odot$. Error bars are estimated to be twice the standard deviation.

SMBH Masses: Directly

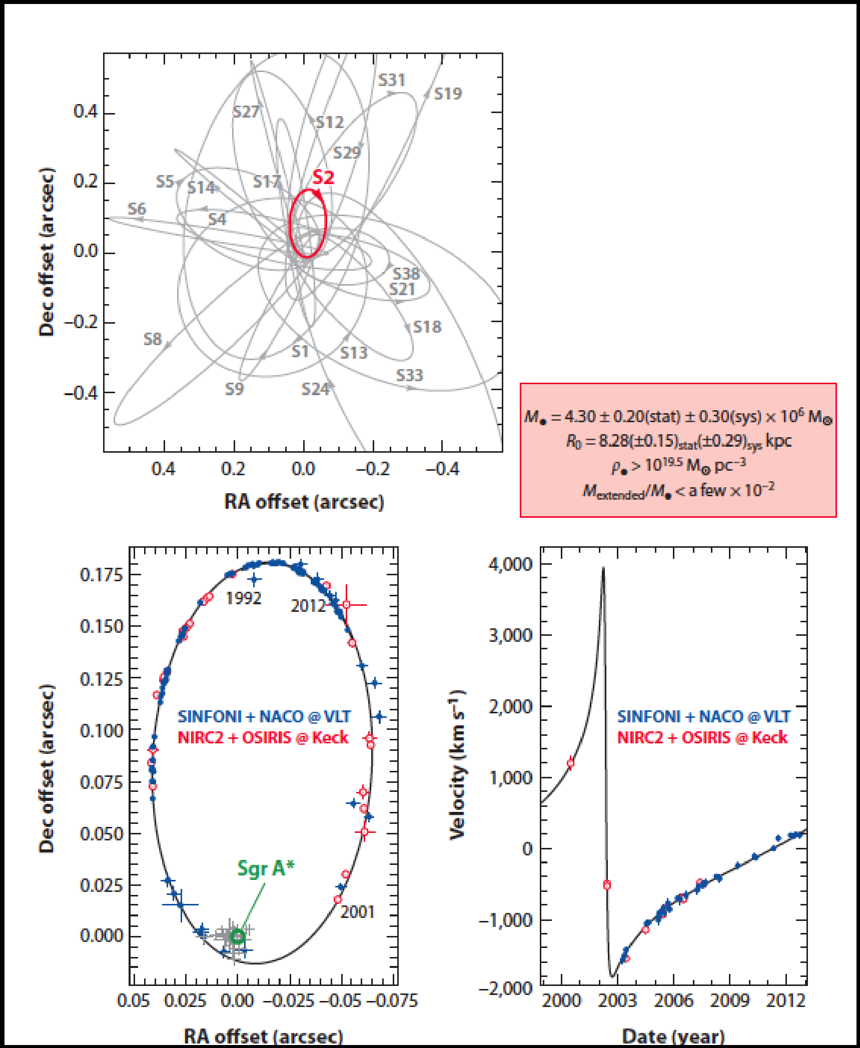

Measuring the mass of the SMBH in our Galaxy through stellar motions.

SMBH Masses: Directly

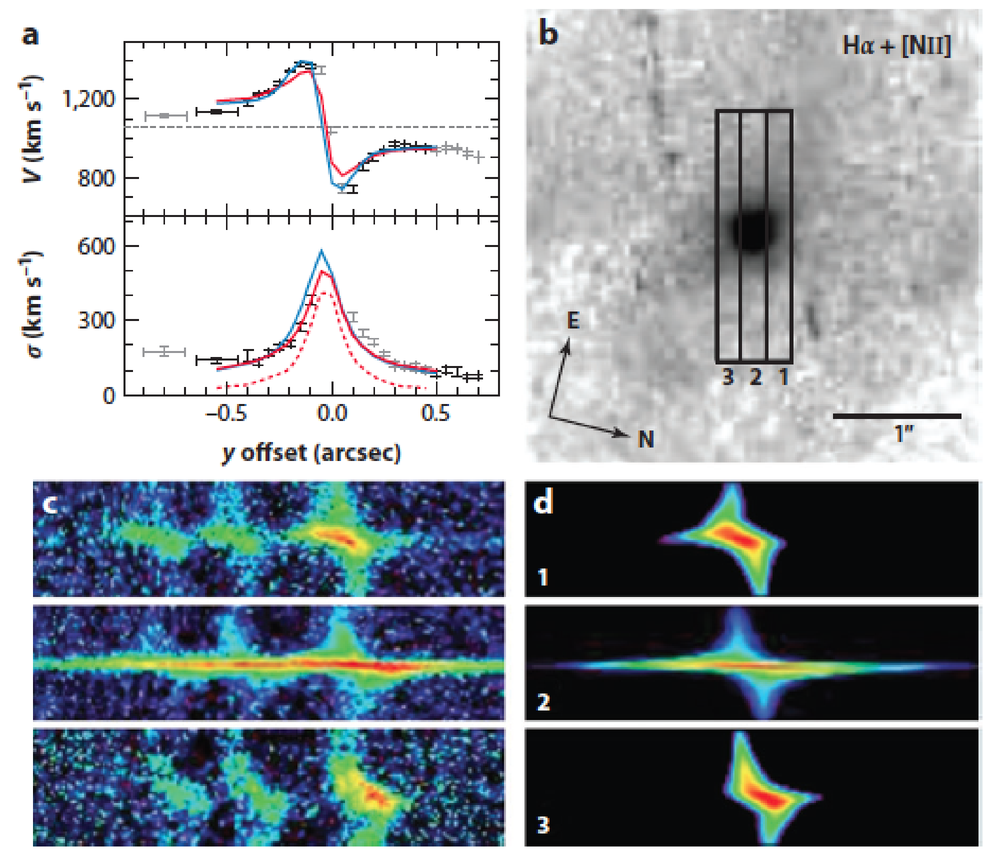

Figure 6

Space Telescope Imaging Spectrograph (STIS) observations of NGC 4374 (Bower et al. 1998) as analyzed by Walsh, Barth & Sarzi (2010). (*b*) WFPC2 continuum-subtracted Hα+[NII] image showing the nuclear disk of ionized gas. The footprints of the three slits are overlaid. (*a*) The radial profiles of [NII] λ 6583 mean velocity and velocity dispersion (in kilometers per second) along the central slit position. Superposed are predictions of the best black hole model with (*blue curve*) and without (*red solid curve*) correction for asymmetric drift. The red dotted curve shows the contribution from rotational line broadening; because these velocity dispersions are smaller than the ones observed, the intrinsic velocity dispersion must be significant. The bottom panels show (*c*) the continuum-subtracted, two-dimensional STIS spectra of the Hα+[NII] region and (*d*) the synthetic spectra of [NII] λ 6583. The vertical axis is the spatial direction, and the horizontal axis shows wavelength increasing toward the right. The three slit positions correspond to the locations labeled in panel *b*.

SMBH Masses: Scaling Laws

$$\frac{M_\bullet}{10^9\,M_\odot} = \left(0.544^{+0.067}_{-0.059}\right)\left(\frac{L_{Ks,\,\mathrm{bulge}}}{10^{11}\,L_{Ks\odot}}\right)$$

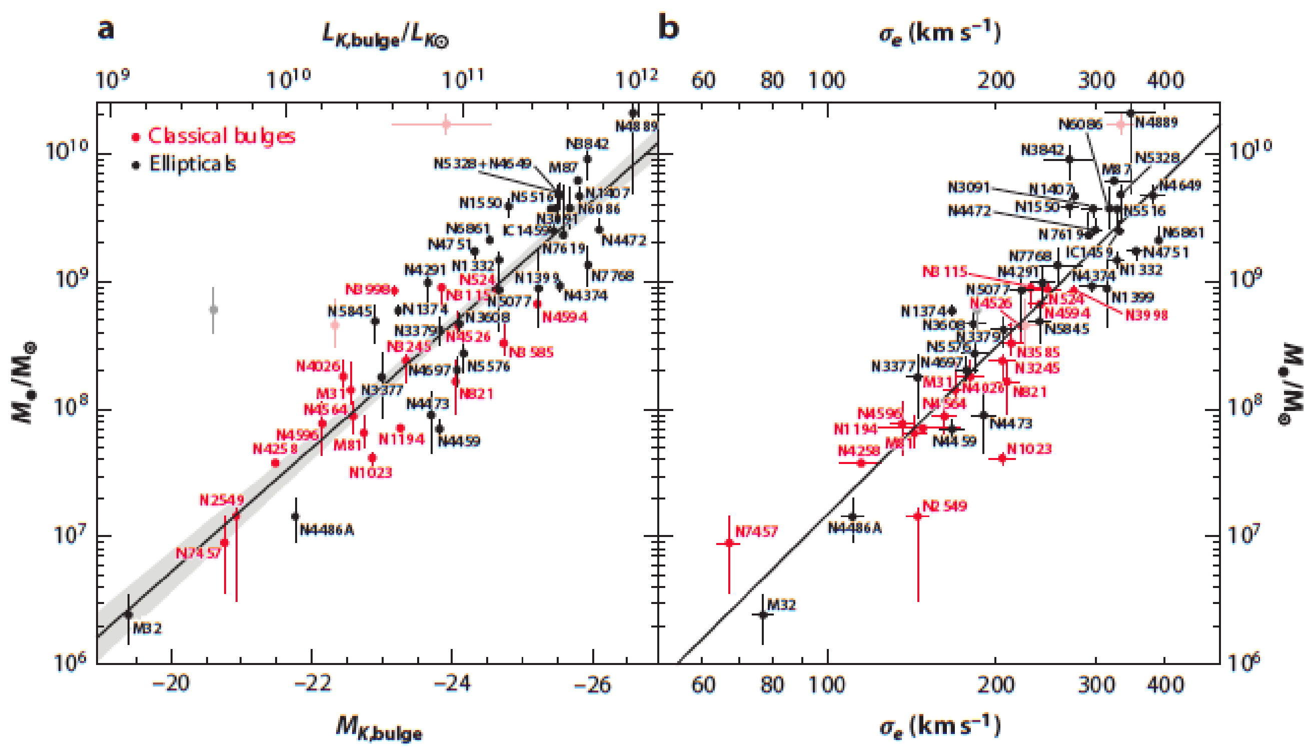

Figure 16

Correlation of dynamically measured black hole mass $M_\bullet$ with (*a*) *K*-band absolute magnitude $M_{K,\mathrm{bulge}}$ and luminosity $L_{K,\mathrm{bulge}}$ and (*b*) velocity dispersion σ_e for (*red*) classical bulges and (*black*) elliptical galaxies. The lines are symmetric least-squares fits to all the points except the monsters (*points in light colors*), NGC 3842, and NGC 4889. Figure 17 shows this fit with 1-σ error bars.

$$\frac{M_\bullet}{10^9\,M_\odot} = \left(0.310^{+0.037}_{-0.33}\right)\left(\frac{\sigma}{200\ \mathrm{km\,s^{-1}}}\right)^{4.38\pm0.29}$$

The surface brightness profile of Holm 15A

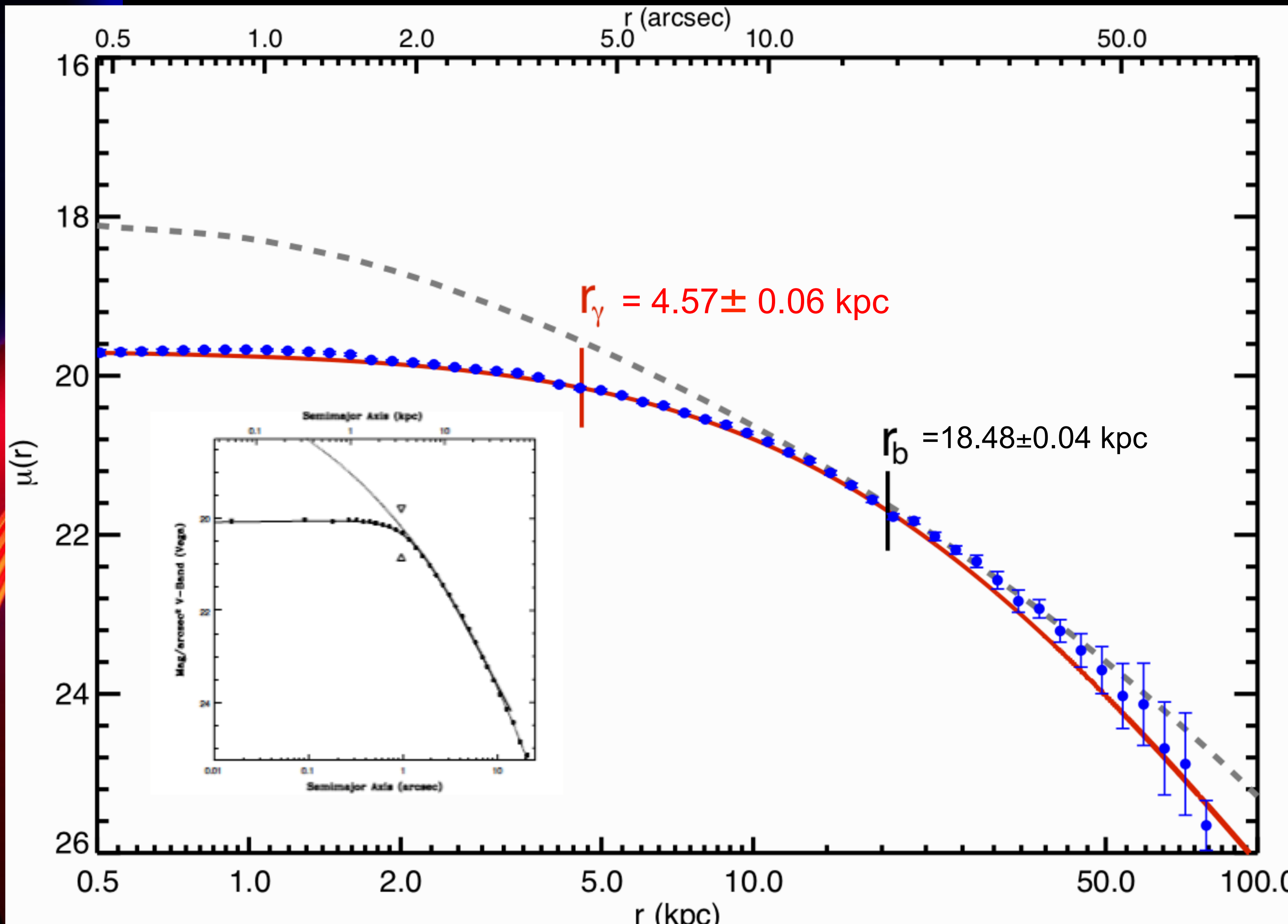

Missing light correlates with BH mass (Kormendy & Bender 2009; Kormendy & Ho 2013)

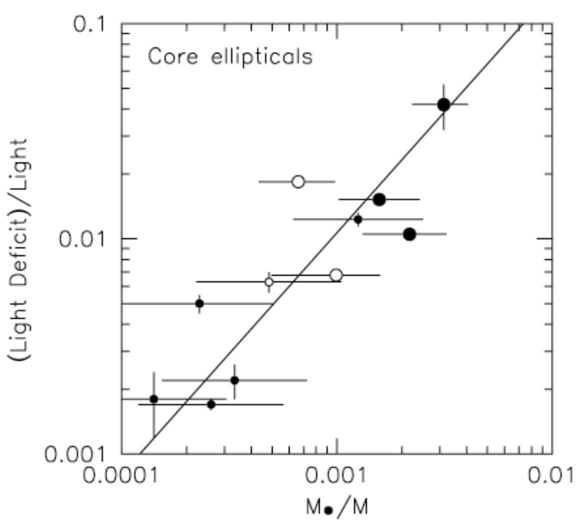

Figure 2. Fraction of the total *V*-band luminosity "missing" in cores vs. the ratio of BH mass to the total stellar mass of the galaxy. The sample is as in Figure 1 and Table 1. Large and small symbols denote galaxies with and without dynamical BH detections. The galaxies with BH detections are (top to bottom) M87 (Macchetto et al. 1997), NGC 4261 (Ferrarese et al. 1996), NGC 4374 (Bower et al. 1998), NGC 4649 (Gebhardt et al. 2003), and NGC 3379 (Gebhardt et al. 2000a). The line is Equation (1).

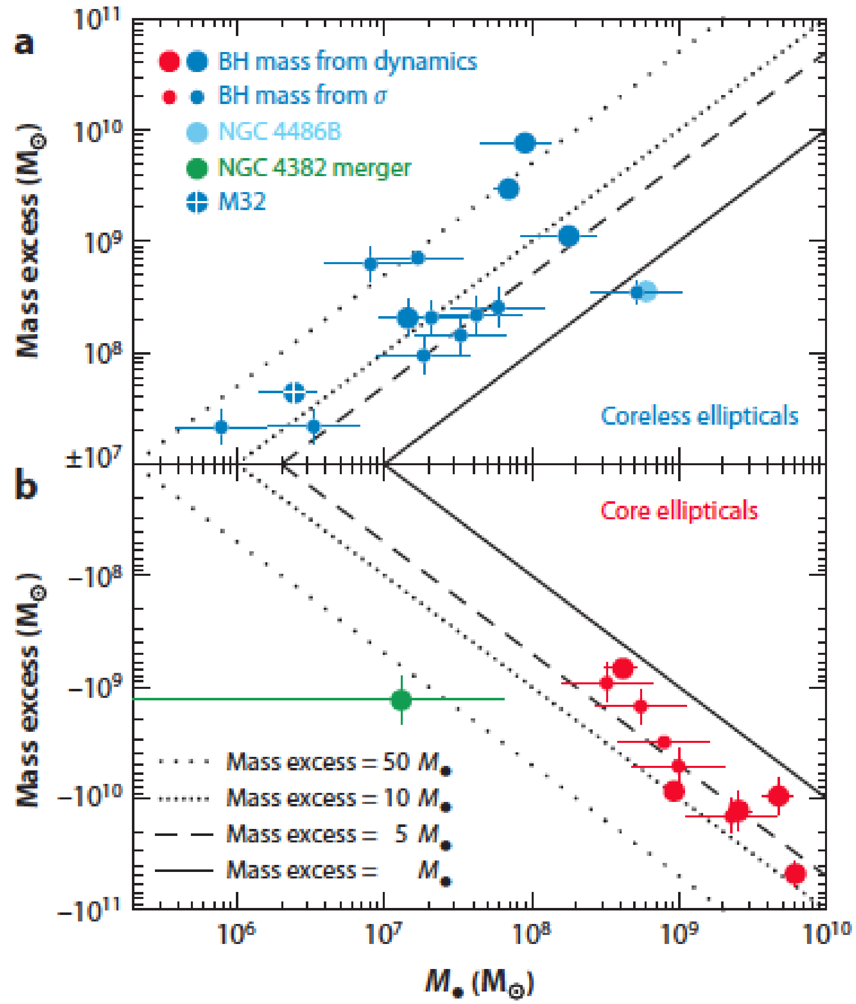

$$\frac{M_\bullet}{10^8\,M_\odot} = \left(0.81^{+0.18}_{-0.15}\right)\left(\frac{L_{V,\,\mathrm{def}}}{L_{V\odot}}\right)^{0.95^{+0.18}_{-0.13}}$$

'extra" in coreless galaxies or (*b*) "missing" in cores versus black hole (BH) mass. Large galaxies with dynamical $M_\bullet$ measurements; small ones use $M_\bullet$ given by the $M_\bullet$-σ relation. ts correlate with BH mass: $M_{\mathrm{def}} \simeq 4M_\bullet$. Mass excesses tend to be larger than mass deficits re scatter with $M_\bullet$. It is important to note that the merger in progress NGC 4382 has a its luminosity but deviates to small $M_\bullet$. If cores are excavated by BH binaries, this suggests oes not lack a big BH (or BH binary) but rather that this BH (or BH binary) is not resident at the center. Updated from Kormendy & Bender (2009).

Rusli et al. 2013

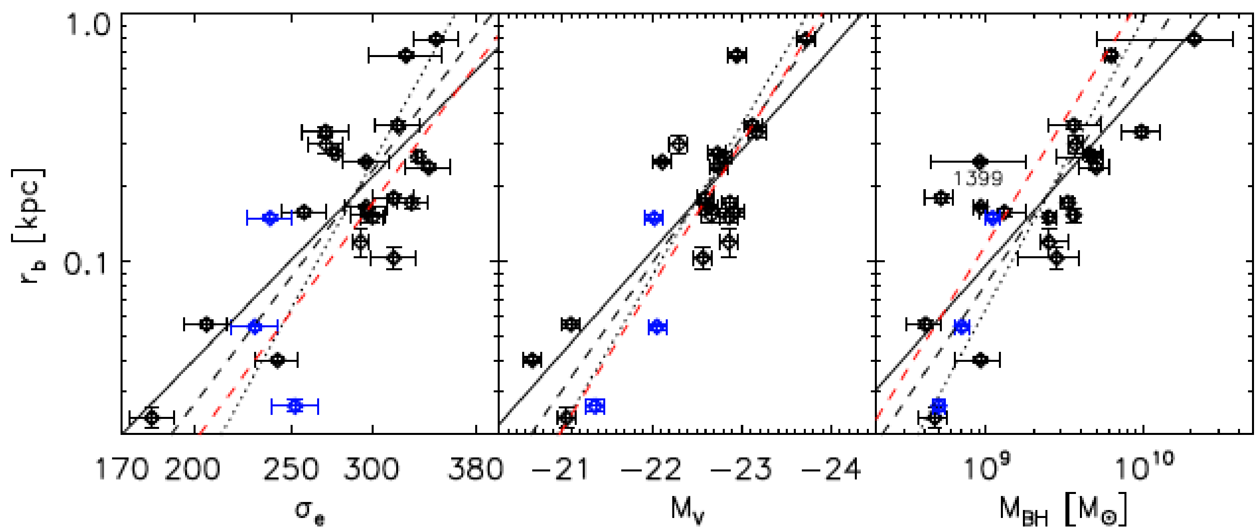

Fig. 7.— From left to right: the break radius is plotted as a function of velocity dispersion within the effective radius σ_e, luminosity of the host galaxy and black hole mass. The 20 galaxies with reliable $M_{\rm BH}$ are represented by the black diamonds. The additional three galaxies without reliable $M_{\rm BH}$ (NGC 4552, NGC 5813, NGC 5846) are shown in blue. The black lines show our fits to all black datapoints. The solid lines show the fits when x-axis variables are treated as independent variables/predictors, the dotted lines are fits when these parameters are the response, and the dashed lines represent the symmetrical bisector regression; see Table 5. The red dashed lines are the bisector fits from Dullo & Graham (2012), i.e. their equations 5, 6, and 12, respectively.

$$\log\left(\frac{\mathrm{M}_\bullet}{3\times10^{9}\,\mathrm{M}_\odot}\right) = (0.59 \pm 16) + (0.92 \pm 0.20)\log\left(\frac{r_b}{\mathrm{kpc}}\right)$$

Lauer et al. 2007

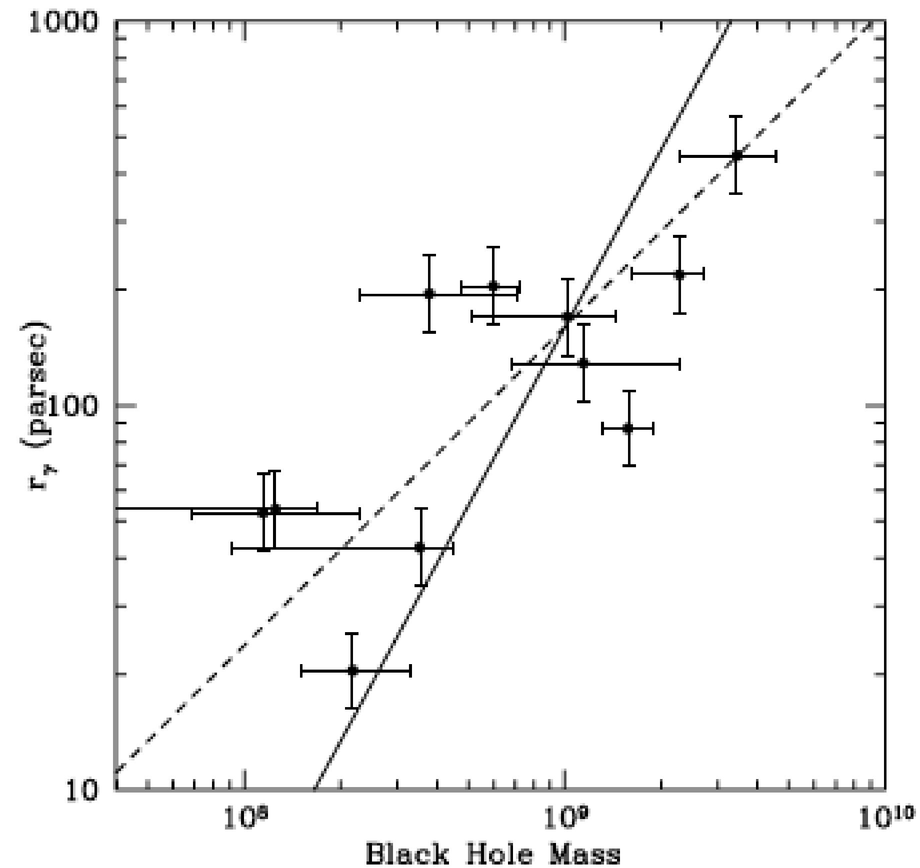

FIG. 7.—BH mass vs. core size, r_γ, for the 11 core galaxies that have $M_\bullet$ measurements. The dashed line is the symmetric fit between $M_\bullet$ and r_γ provided by eq. (24), while the solid line gives the fit presented in eq. (25), which assumes that r_γ is the independent variable. [*See the electronic edition of the Journal for a color version of this figure.*]

$$\log\left(\frac{r_\gamma}{\mathrm{kpc}}\right) = (0.59 \pm 0.18)\log\left(\frac{\mathrm{M}_\bullet}{10^9\,\mathrm{M}_\odot}\right) + (2.19 \pm 0.10)$$

How Big the SMBH in Holm 15A?

Table 2. Holm 15A: Black Hole Mass Estimates

Relation	$M_\bullet$ $[M_\odot]$	Reference
$M_\bullet - \sigma$	$\sim 2.1 \times 10^9$	Kormendy & Ho (2013, Eqs. 6)
$M_\bullet - L_{K,bulge}{}^*$	$\sim 9.2 \times 10^9$	Kormendy & Ho (2013, Eqs. 7)
$M_\bullet - L_{V,def}$	$\sim 2.6 \times 10^{11}$	Kormendy & Bender (2009, Eq. 3)
$M_\bullet - r_b$	$\sim 1.7 \times 10^{11}$	Rusli et al. (2013, Eq. 13)
$M_\bullet - r_\gamma$	$\sim 3.1 \times 10^{11}$	Lauer et al. (2007, Eq. 26)

*Taking the entire galaxy as a classical bulge, and correcting the value of H_0

How Big the SMBH in Abell 85 Dark Matter Halo?

$$\frac{M_\bullet}{10^8 M_\odot} = 0.168 \left(\frac{V_{circ}}{200\ \mathrm{km\,s^{-1}}} \right)^{5.45}$$

$\sigma_{cl} = 752 \pm 34\ \mathrm{km\,s^{-1}}$, $V_{circ} = \sqrt{2}\sigma_{cl}$;

hence, the mass of the SMBH for Abell 85 DM halo is :

$$M_\bullet \sim 1.5 \times 10^{11}\ M_\odot$$

SMBH Dynamical Effects

$$r_f = \frac{GM_\bullet}{\sigma^2}\,(\text{Influence radius});$$

$$\mathrm{M}_\bullet = 10^{10}\ \mathrm{M}_\odot \text{ and } \sigma \approx 310\,\mathrm{km\,s^{-1}}:$$

$$r_f \sim 450\,\mathrm{pc}\ (0.42'')$$

Holm 15A is a LINER

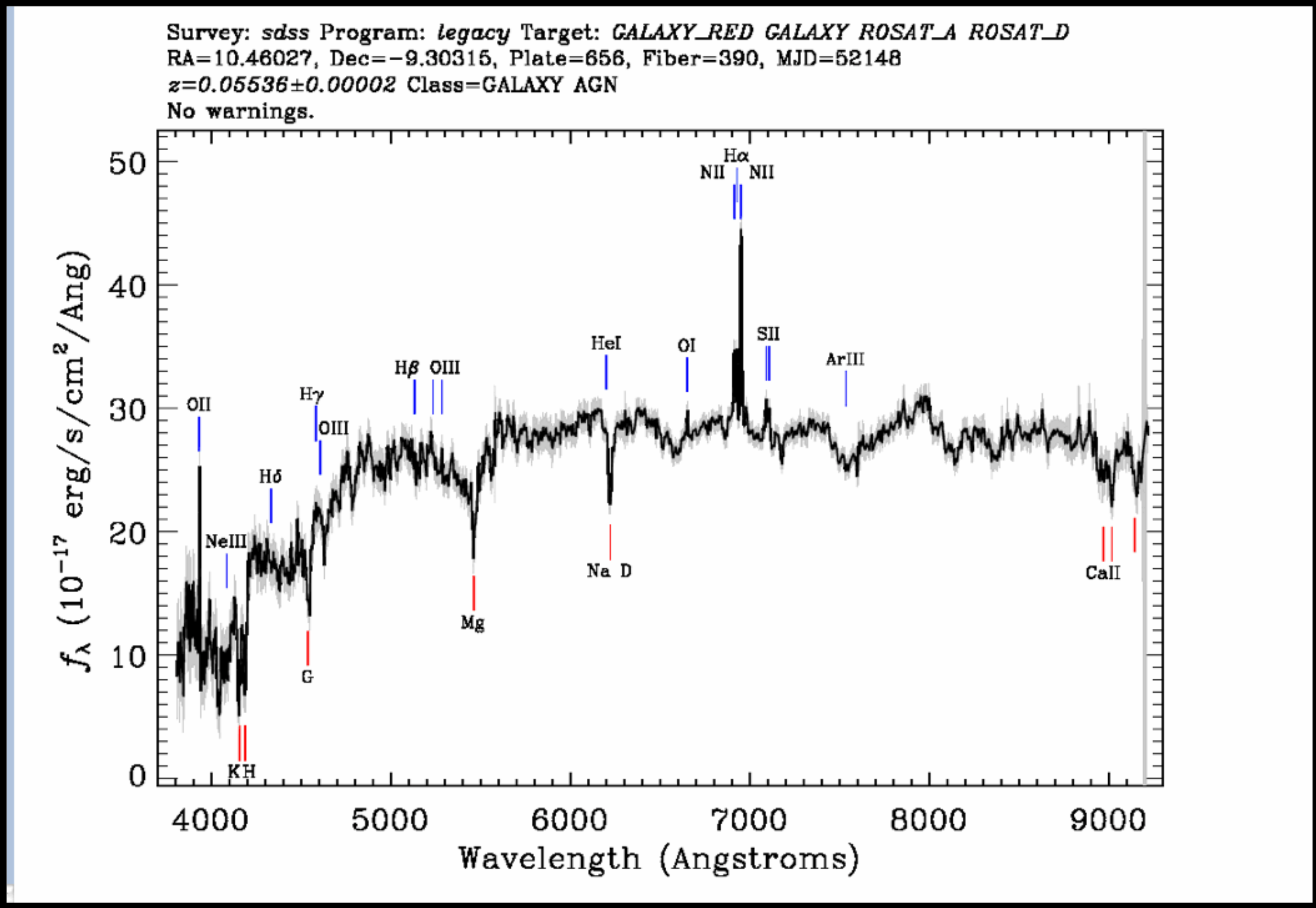

Cores are explained by the scouring action of Supermassive Binary Black Holes (SBBH).

Is there a SBBH in HOLM 015A? Maybe…

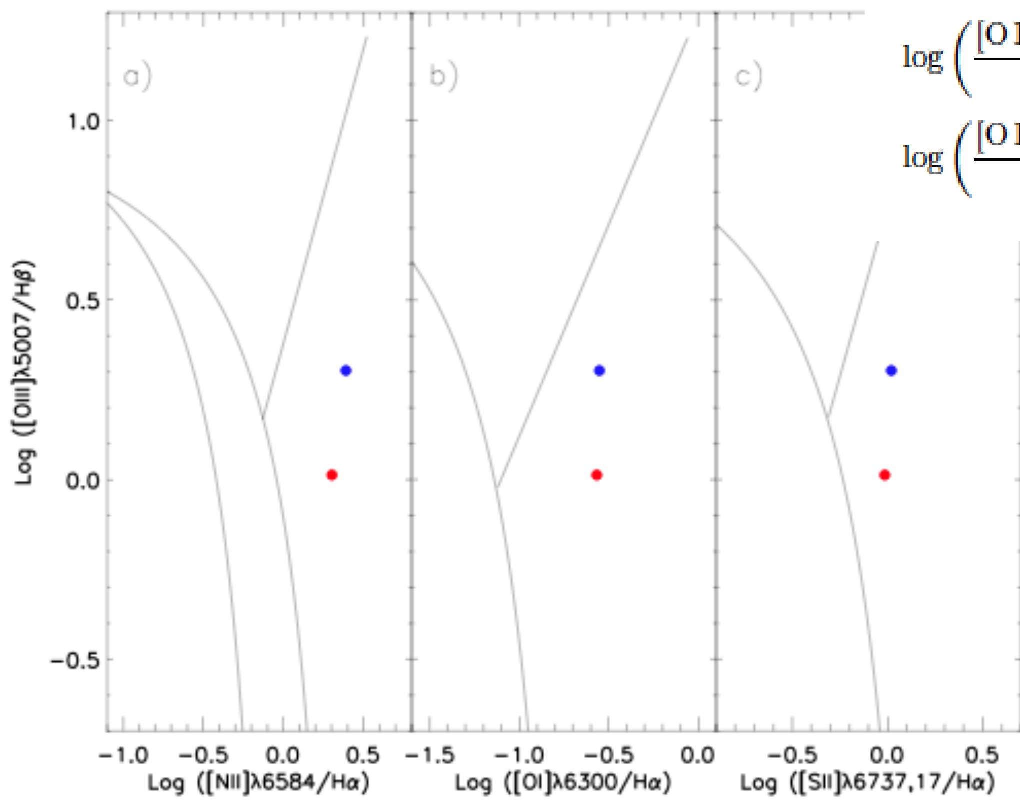

$$\log\left(\frac{[\mathrm{O\,III}]\lambda 5007}{\mathrm{H}_\beta}\right) = 0.013,\ \log\left(\frac{[\mathrm{N\,II}]\lambda 6584}{\mathrm{H}_\alpha}\right) = 0.302;$$

$$\log\left(\frac{[\mathrm{O\,I}]\lambda 6300}{\mathrm{H}_\alpha}\right) = -0.567, \log\left(\frac{[\mathrm{S\,II}]\lambda 6737.17}{\mathrm{H}_\alpha}\right) = -0.014.$$

A2261-BGC doesn’t show emission lines.

Are there SMBH binaries?

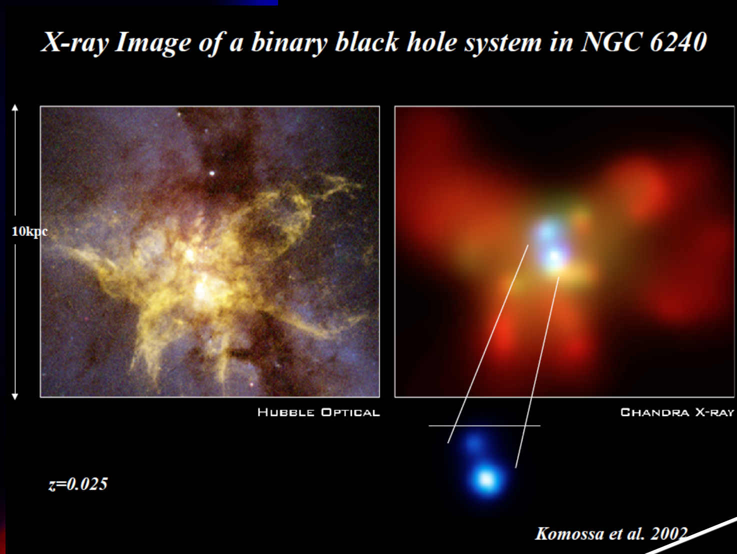

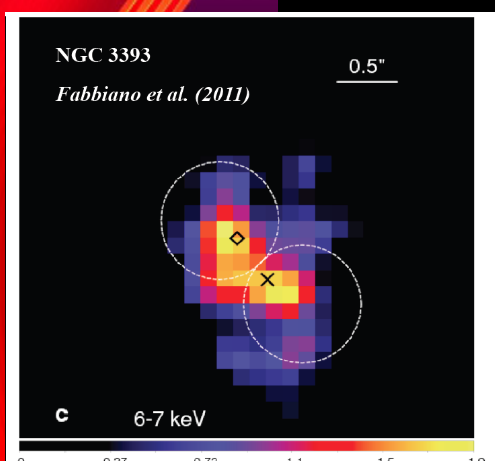

SMBM binary

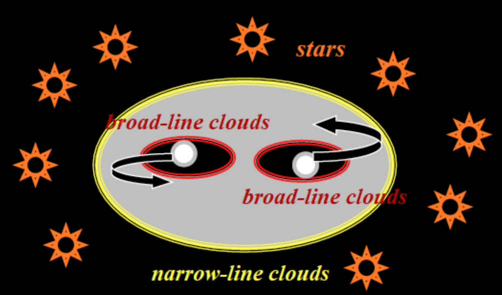

SDSS images & spectra of selected double narrow -line quasars

(Liu et al. 2009)

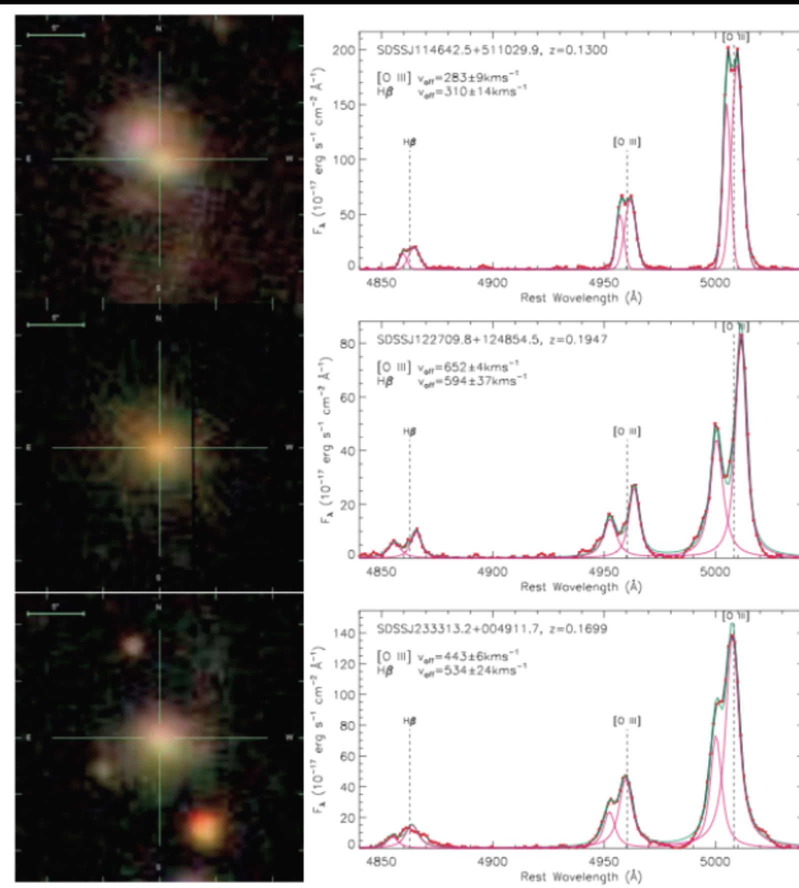

But Holm 15A has no double narrow-lines

Is there a SMBH binary?

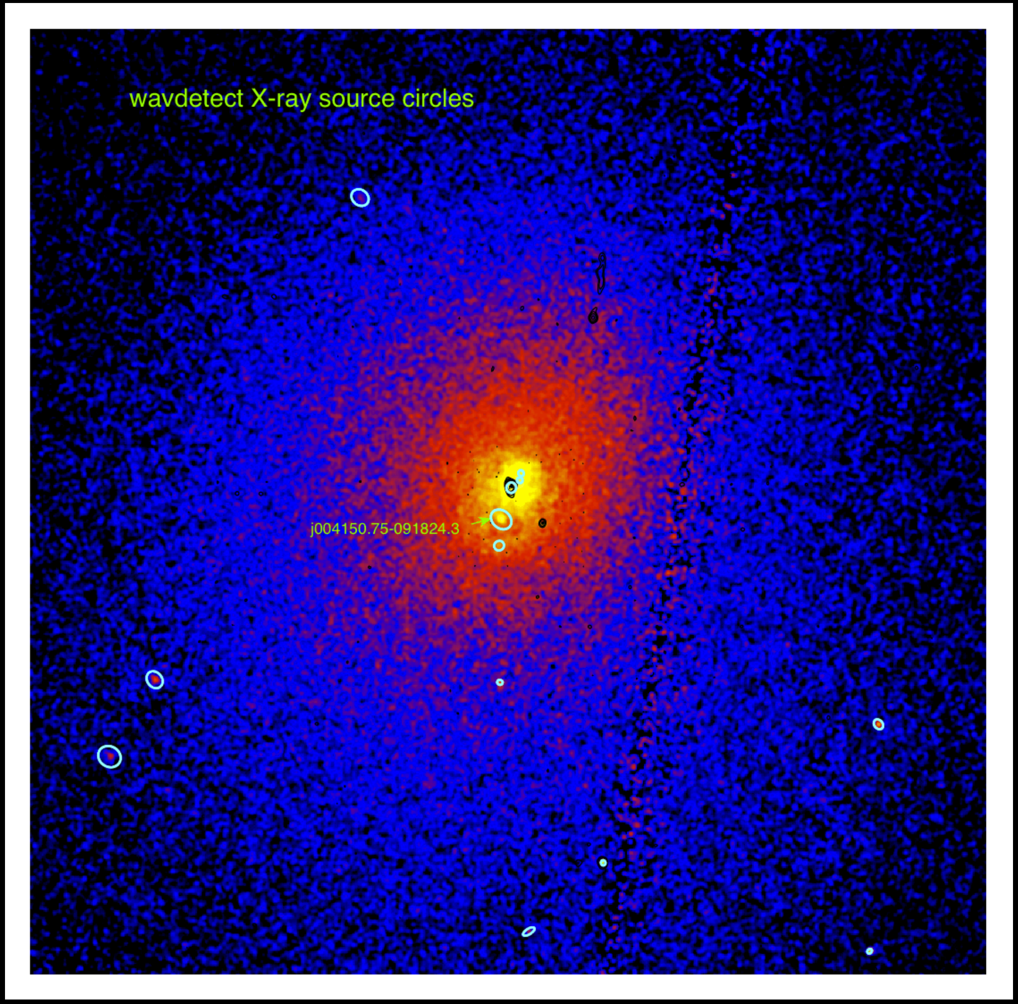

Holm 15A

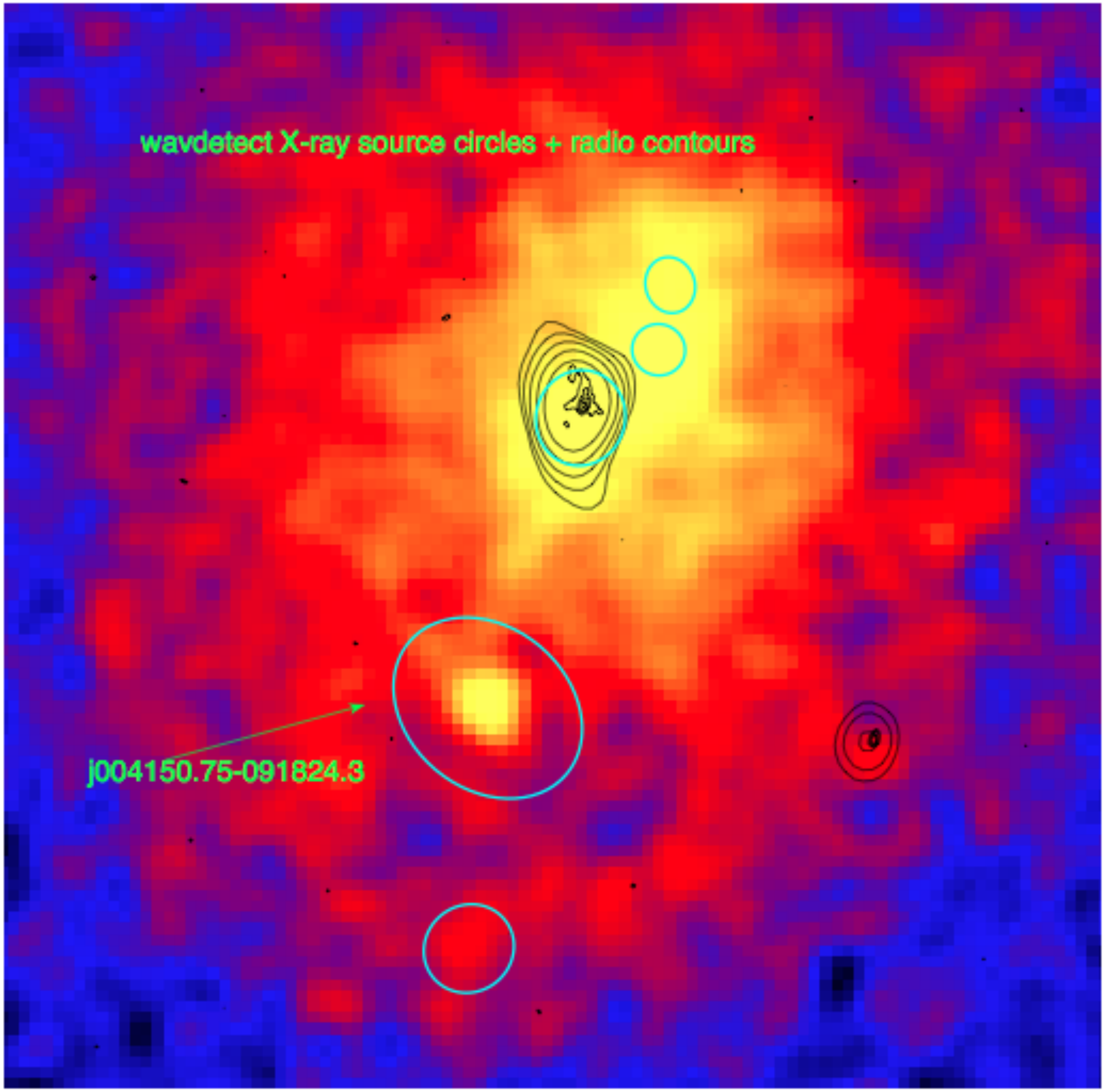
wavdetect X-ray source circles + radio contours
j004150.75-091824.3

Holm 15A

Maybe: A candidate supermassive binary black hole system in the brightest cluster galaxy of RBS 797 (z~0.35) reported by Gitti and collaborators 2014

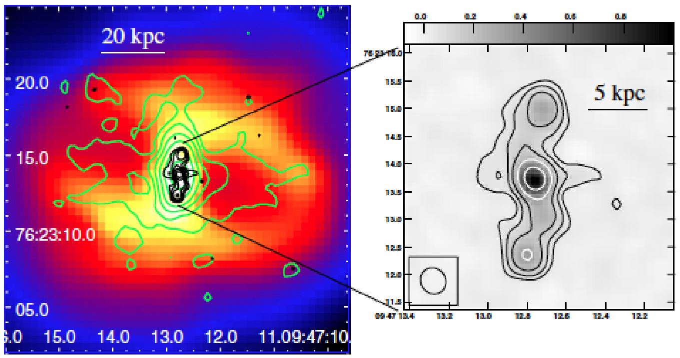

Fig. 2. The 4.8 GHz VLA contours obtained from the combined A- and B-array archival observations of RBS 797, imaged at different resolutions, are overlaid onto the *Chandra* image of the central region of the cluster (*left panel*). Green contours: 4.8 GHz VLA map at 1″.38 × 1″.33 resolution, obtained by setting ROBUST=+5, UVTAPER=250; the rms noise is 0.01 mJy beam^{-1} and the contour levels are 0.03, 0.06, 0.12, 0.24, 0.48, and 0.96 mJy beam^{-1}; the total flux density is ~4 mJy, with a peak flux density of 1.5 mJy beam^{-1}. Black contours (best visible in the zoom in the *right panel*): 4.8 GHz VLA map at 0″.49 × 0″.44 resolution, obtained by setting ROBUST=0, UVTAPER=0; the rms noise is 0.01 mJy beam^{-1} and the contour levels are 0.04, 0.08, 0.16, 0.32, and 0.64 mJy beam^{-1}; the total flux density is ~2.8 mJy, with a peak flux density of 1.0 mJy beam^{-1}.

EVN observations. 56 minutes on source

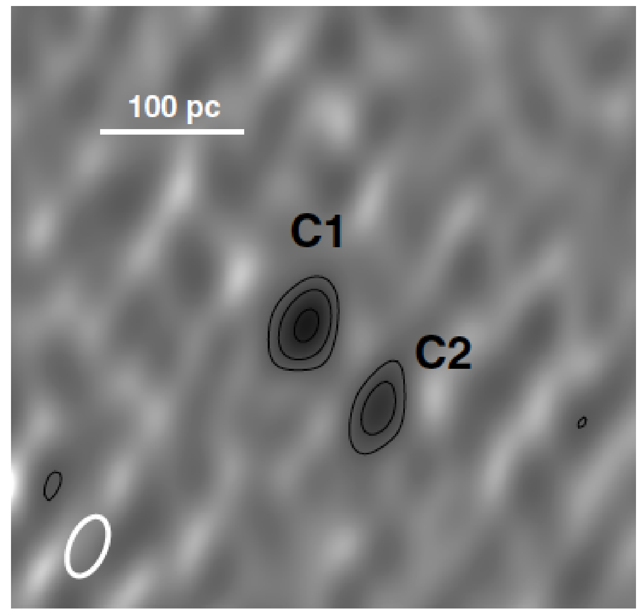

Fig. 1. 5 GHz EVN map of the BCG in RBS 797 at a resolution of 9.4×5.3 mas^2 in PA −24° (the beam is shown in the lower-left corner). The rms noise is 36 μJy beam^{-1} and the peak flux density is 0.53 mJy beam^{-1}. The contours levels start at 3σ and increase by a factor of 2. Two components, separated by 16 mas (~77 pc), are clearly detected.

Gitti et al. 2014

The Eddington Limit

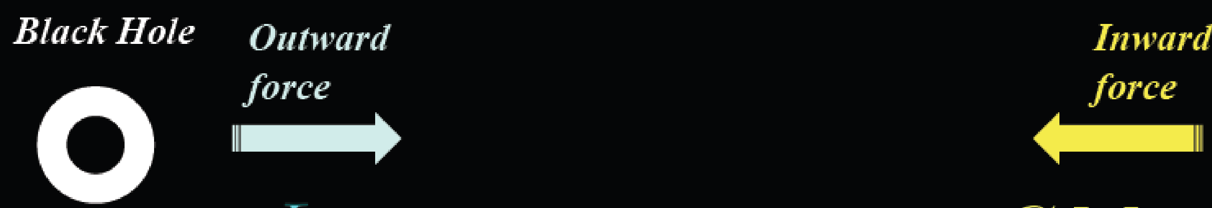

$$\frac{L}{4\pi r^2 c}\sigma_T \qquad \qquad \frac{GMm_p}{r^2}$$

$$L_E = \frac{4\pi G M m_p c}{\sigma_T} = 1.3 \times 10^{38} \frac{\text{erg}}{\text{s}} \left(\frac{M}{M_\odot} \right).$$

Black Hole Growth

$$L = \epsilon \dot{M} c^2 = \eta L_E \propto M$$

$$M = M_0 \exp\{t/t_E\}$$

$$t_E = 4 \times 10^7 \left(\frac{\epsilon/\eta}{10\%} \right) \text{years}$$

Starting from a stellar mass, there is barely enough time to grow the observed quasar black hole during the age of the Universe at z=7.1 for e=10%… but the radiative efficiency may be small due to trapping of radiation:

$$v_{\rm diff} \sim (c/\tau) \ll v_{\rm infall}$$

How about the brightest cD in the local universe?

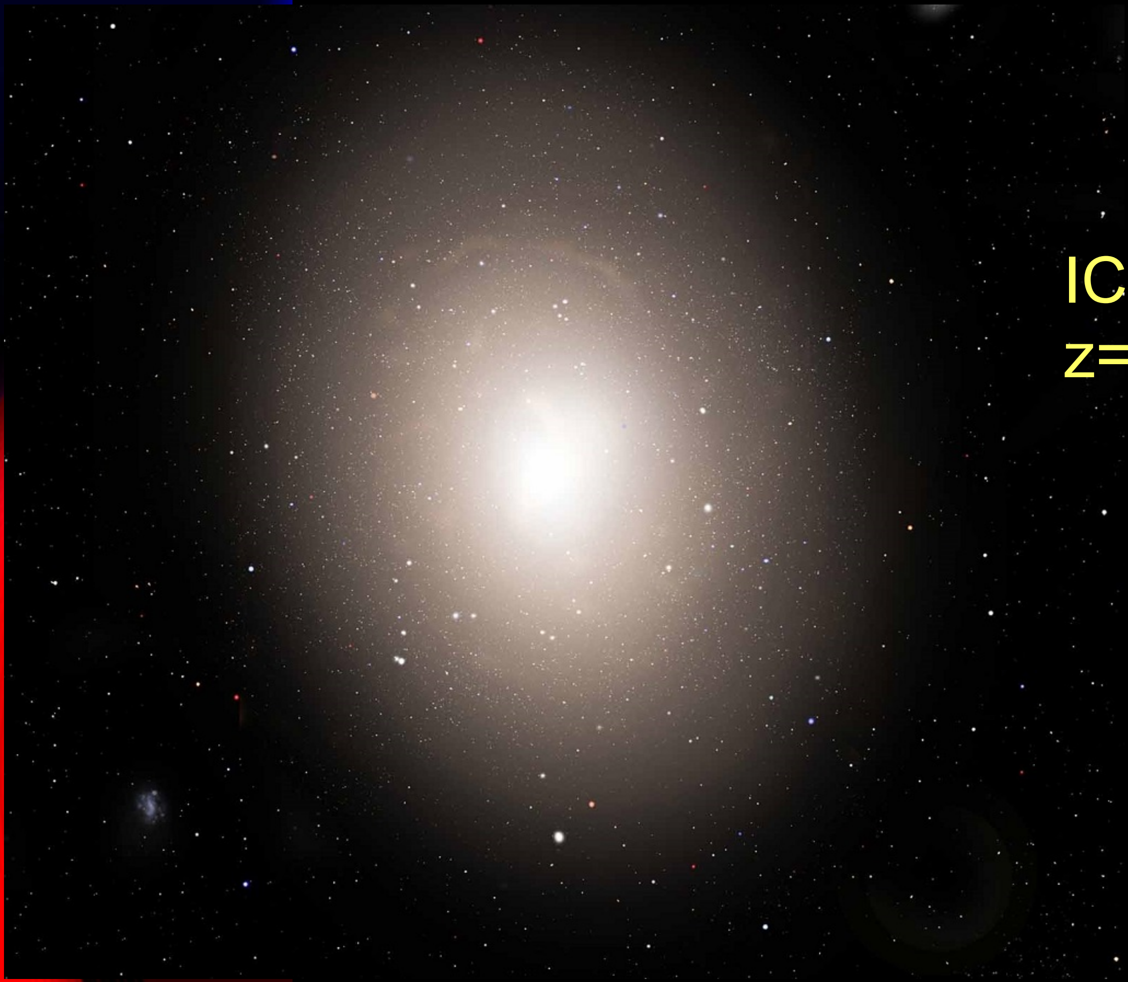

IC 1101 in Abell 2029,
z=0.077947

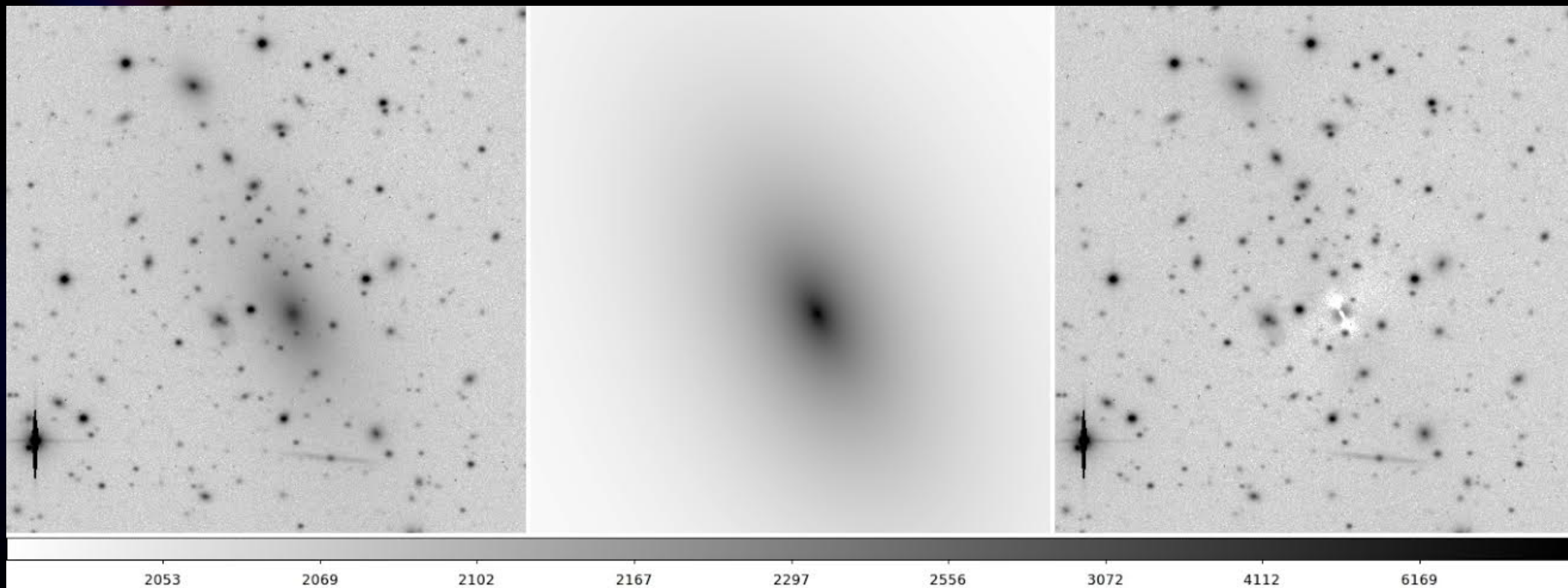

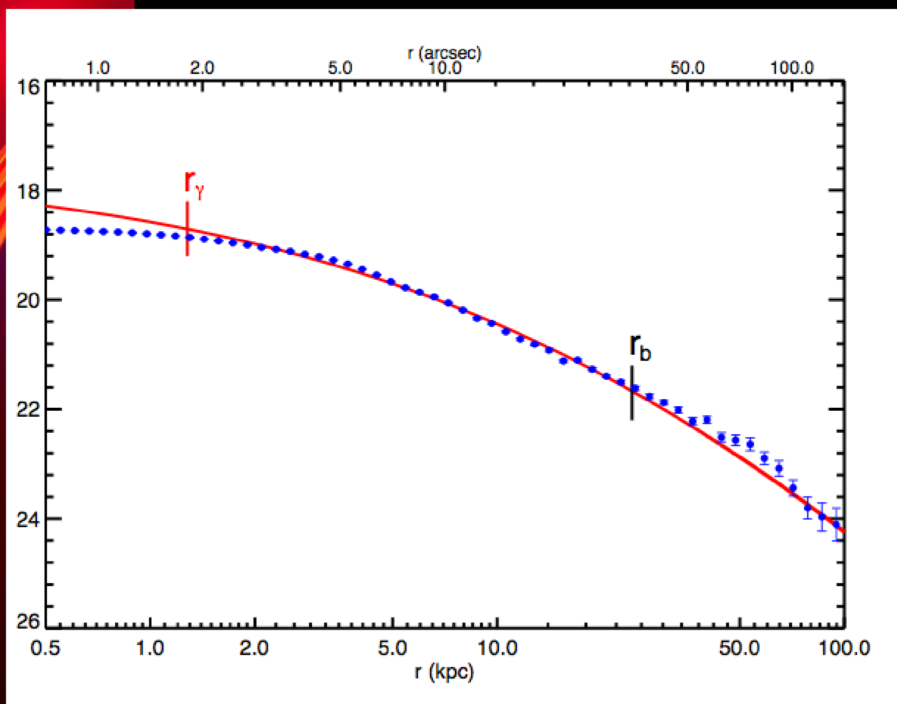

IC 1101

$$r_\gamma \sim 1.3\,\mathrm{kpc}$$

IC 1101 breaks away

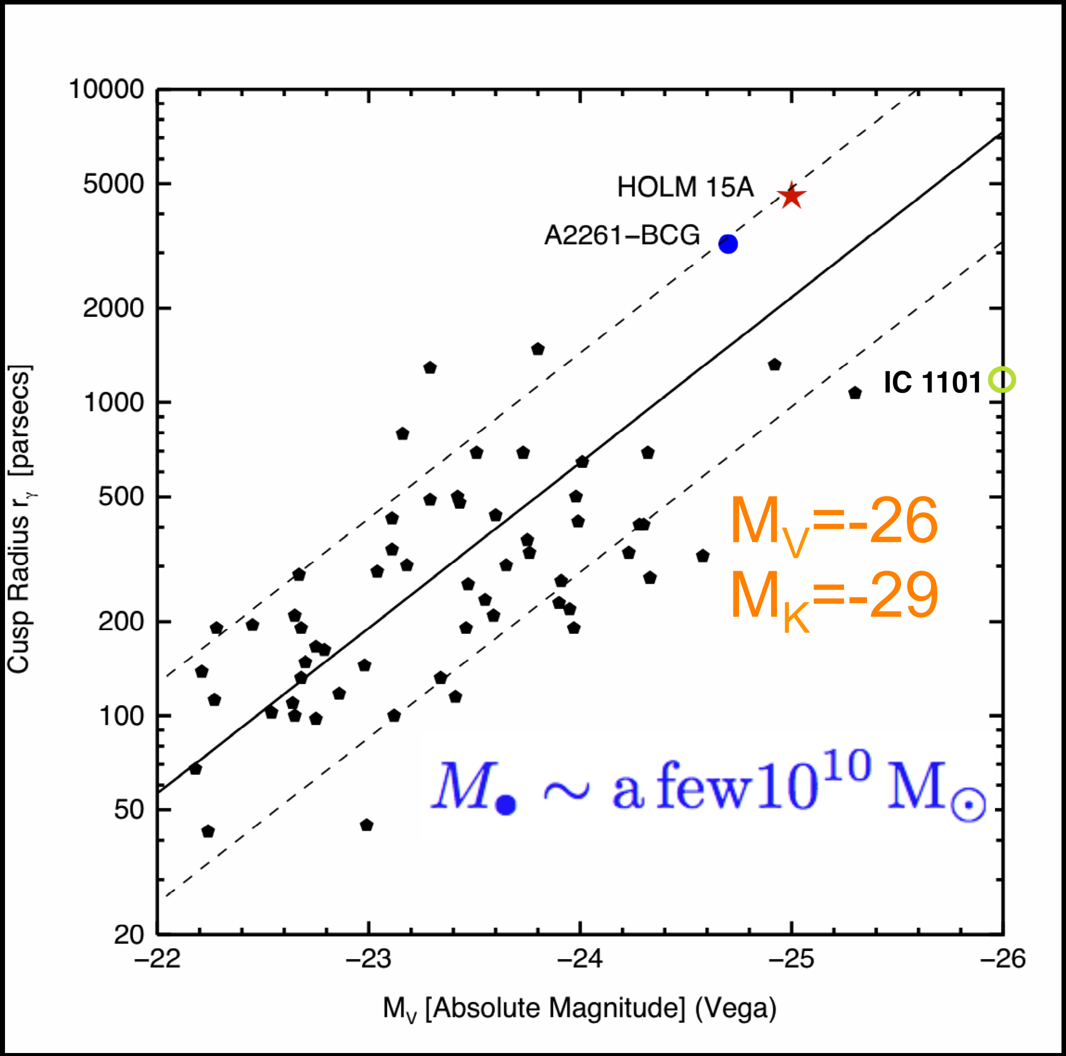

Conclusions

We have found that Holm 15A has the largest core known so far. A central AGN supports the presence of a central BH, which could be ultramassive ~ 10^{10} M_{sun}. This seems to be a limit for maximum BH growth. Very large cores seem to be rare and may represent a relatively brief phase in the evolution of BCG, as the merging times for SMBH binaries should be relatively short (Kahn et al. 2014). After SMBH binary merger cusp regeneration would induce core shrinkage (Merritt 2006). If SMBH growth is regulated by galaxy mergers (e.g., Merritt 2006, Booth & Schaye 2011), their final masses were set, perhaps, by initial conditions (e.g., Treister et al 2013).

Holm 15A presents the best conditions to explore the effects of SMBH. We are proposing follow up observations (i.e., detection of BH gravitational lens using the background of SMG). I did not mention gravity waves nor dark mater annihilation …

López-Cruz, O., Añorve, C., Birkinshaw, M., et al. ApJ , 795, L31

Desde el 15 de octubre de 2014, estamos en las noticias en el mundo.

México (Excélsior), Guatemala, Perú, Colombia, Chile, Argentina, Brasil, España (El País).

También en radio y televisón.

Recientemente (6 de noviembre), New Scientist, una de las revistas de divulgación de la ciencia más importante en el mundo.

15 de noviembre, 2015, Conozca Más

Estes el cúmulo de Abell 85 en el espectro visible

Fotografía de Abell 85 desde el Kitt Peak National Observatory en Arizona

Fotos: Omar López Cruz

En el artículo "¿En verdad existen los hoyos negros?" (de la edición anterior), el astrónomo y divulgador británico Marcus Chown expone qué es un agujero negro, cómo se han clasificado, además de las ideas que hay en torno de estos cadáveres de estrellas supergigantes. Te invitamos a leerlo para conocer más del tema.

El equipo estadounidense había estudiado a Holm 15A y no le dio importancia. **¡Se les fue el descubrimiento!**

HISTORIA DE UN DESCUBRIMIENTO ENORME

Curiosamente, las circunstancias de este -literalmente- gigantesco hallazgo son peculiares: no sólo requirió varios años, sino también un descuido por parte de astrónomos de EUA. En 1995, Omar López realizaba sus estudios de doctorado en la Universidad de Toronto, donde tuvo su primer contacto con la galaxia Holm 15A. En una parte de sus observaciones astronómicas de 1993, detectó que esta galaxia era peculiar, ya que tenía un bajo brillo superficial, pero no logró más debido a la falta de factores de comparación que le permitieran llegar a datos precisos, además de que las herramientas de análisis eran aún inmaduras.

Para el 2012, los astrónomos estadounidenses Marc Postman y Tod Lauer, junto con un equipo de 15 investigadores dedicados a cazar estallidos de supernova en galaxias, y usando como herramienta al telescopio espacial Hubble, detectaron en la galaxia más brillante en el cúmulo Abell 2261 A2261-BCG, un agujero negro masivo, el más grande descubierto hasta entonces. Este anuncio hizo retomar la investigación de López Cruz debido a que las características descritas por ellos se asemejaban a las que él había estudiado en sus años en Toronto. Y las circunstancias, a poco más de una década después, permitieron al investigador del INAOE tener las herramientas suficientes para avanzar en el estudio de Holm 15A.

A cada integrante del equipo que conjuntó (mencionado en la entrevista con él) le asignó una tarea en específico, ya que la investigación de la galaxia requirió de utilizar datos de su propia tesis doctoral e imágenes de diferentes telescopios ubicados en el espacio y en tierra, y procesarlas en supercomputadoras que corrían programas escritos especialmente para atender este estudio.

El esfuerzo colaborativo de los científicos y la tenacidad del Dr. Omar López mostró un resultado impresionante: en el centro de la galaxia Holm 15A vive un agujero negro con una escala descomunal, mucho más grande que el de la A2261-BCG. ¡Y así estos investigadores encontraron el mayor hoyo negro jamás hallado!

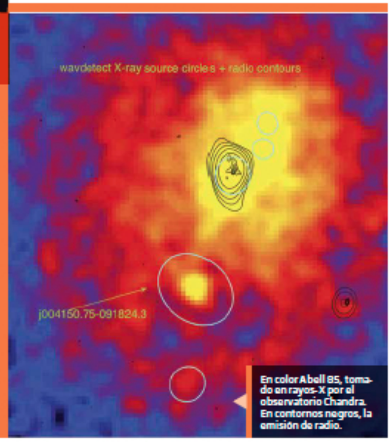

En color Abell 85, tomado en rayos-X por el observatorio Chandra. En contornos negros, la emisión de radio.

DR. OMAR LÓPEZ CRUZ, DEL INAOE

De primera mano, el investigador en jefe del proyecto nos explica todo lo relacionado a este importante descubrimiento astronómico.

CM ¿CÓMO SE HIZO ESTE DESCUBRIMIENTO?
Dr. Omar López Cruz: Es un proceso bastante largo. Desde 1995 nos dimos cuenta de que la galaxia central, la más brillante de Abell 85 [Abel es un cúmulo de galaxias], a la que llamamos Holm 15A , tenía la peculiaridad de ser de muy bajo brillo superficial. Es decir, que en lugar de estar concentrada hacia el centro, era difusa. ¡Incluso llegamos a decir que era 'esponjadita'! Aunque ya en 1980 un colega había reportado que ésta tenía propiedades especiales, no sabíamos cuáles eran. No teníamos referente. Entonces, gracias a un programa nuevo dirigido por mis colegas Postman y Lauer, usando el telescopio espacial Hubble, equipado ahora con una cámara especial para abarcar un área grande del Universo y así buscar supernovas en galaxias –particularmente querían establecer la tasa de supernovas en galaxias elípticas–, se descubrió que en la galaxia Abell 2261-BCG existía un aplanamiento en el centro, y la declararon como la de mayor núcleo ('core', en inglés) que jamás se haya medido. Este 'aplanamiento' se cree que se debe a la interacción de dos agujeros negros binarios.

Por las leyes de escalamiento que aplicamos, inferimos que entre mayor sea dicho core, mayor será el agujero negro en la galaxia. Pero no se detectó ninguna firma de un agujero negro binario, ni actividad de AGN [ver recuadro] por el espectro, ni gas en A2261-BCG. Y entonces nos acordamos de Abell 85.

Yo no la quise medir. Le di los datos a mi estudiante Christopher Añorve. Su trabajo es muy importante, ya que él llevó a cabo un programa de ajuste de brillo superficial. Así, ya teníamos la herramienta hecha. Él me dio los resultados para interpretarlos y vimos que Holm 15A era mucho mayor que Abell 2261-BCG.

ERES EL AUTOR PRINCIPAL DE LA INVESTIGACIÓN, ¿QUIÉNES SON LOS COLABORADORES QUE MENCIONAS?
Los astrónomos colaboramos con mucha gente. Christopher Añorve, de la Universidad Autónoma de Sinaloa, hizo el ajuste de brillo superficial. M. Birkinshaw analizó los datos en [el espectro de] radio, y D.M. Worrall, en el de rayos X. Ambos provienen de la Universidad de Bristol. Héctor Ibarra Medel, mi estudiante del INAOE, hizo la dinámica del cúmulo. Wayne A. Barkhose, de la Universidad de Dakota del Norte, desarrolló el análisis de una dimensión. Juan Pablo Torres Papaquin, de la Universidad de Guanajuato, realizó el análisis del espectro con el que determinamos que es un tipo de AGN de baja luminosidad. Verónica Motta, de la Universidad de Valparaíso, nos ayudó con la dinámica.

PLATÍCANOS SOBRE EL EQUIPO ESTADOUNIDENSE AL QUE SE LE ESCABULLÓ ESTE DESCUBRIMIENTO.
Marc Postman y Tod Lauer son grandes investigadores que han conducido programas muy importantes en cuanto al estudio de agujeros negros y galaxias elípticas... Ellos y su grupo son el referente en el estudio de agujeros negros. Cuando encontraron y reportaron la galaxia Abell 2261-BCG, se abrió la oportunidad de hacerle justicia a Holm 15A. Eso fue lo que me hizo tener que pensar: "Veamos si es más grande". Como te dije antes, le pedí a Christopher que la midiera para no sesgar dicha medición, porque en el fondo quería que fuera más grande. Así que Christopher la midió y resultó que es mayor por un kiloparsec [ver recuadro "poniéndolo en perspectiva"], es decir, ¡descubrimos un monstruo! Y con eso rompimos el récord establecido en 2012.

PONIÉNDOLO EN PERSPECTIVA

¿Qué es eso de 'kiloparsec' (o kpc)? Simple: es una unidad astronómica para medir la distancia hacia objetos fuera de nuestro sistema solar. Un parsec equivale a aproximadamente 3.26 años luz, por lo que mil pársecs o un kpc son unos 3,260 años luz.

¿QUÉ APORTA ESTE DESCUBRIMIENTO A LA EVOLUCIÓN DE GALAXIAS?
A los agujeros negros de 10^9 veces la masa del sol los llamamos supermasivos. Con esto hablamos de agujeros ultramasivos de 10^{10}. Esto nos dice que quizá los agujeros negros no crezcan más. ¿Por qué? Aún no lo sabemos.

¿QUÉ IMPLICA ESTE TRABAJO PARA LA ASTROFÍSICA NACIONAL?
Que este es el nuevo paradigma en las bases de datos. Para hacer este trabajo sólo usamos datos de mi tesis y todo lo demás, son datos públicos del SLOAN, del telescopio espacial de rayos X Chandra, del observatorio orbital XMM-Newton, también de rayos X, entre otros. El resultado nos dice que aún no hemos explotado las bases de datos públicas y que todavía hay mucho por descubrir.

¿CÓMO TE SIENTES CON TU DESCUBRIMIENTO?
Imagina que tienes un problema que empezó en 1995, que no te lo has quitado de encima en 19 años y de repente lo acomodas. ¡Se siente maravilloso! Es un gran alivio y regocijo, y lo que no anticipamos es que esta noticia trascendiera de esta manera.

¿CUÁL ES EL SIGUIENTE PASO?
Solicitar el telescopio Hubble y el Gran Telescopio de Canarias para hacer un estudio dinámico.

IN BRIEF

On tameness and tail-dropping in island lizards

LIZARDS are famed for a rather extreme escape tactic – they shed their tails to avoid predation. But for Erhard's wall lizard, found across Greece's Cyclades islands, its tendency to jettison the tail – and indeed its tolerance for disturbance – depends on which island it lives on.

The Cyclades became isolated from each other more than 11,000 years ago. That stranded each island's lizards, marooning them alongside different predators. As a result, the lizards, *Podarcis erhardii*, have been walking different evolutionary paths. Kinsey Brock of the University of Michigan, Ann Arbor, tested the lizards' fear factor by walking towards 813 individuals from 57 islands plus the mainland. The average lizard ran when Brock got within 1.8 metres, but some let her get to 10 centimetres.

She found a link between the distance at which a lizard flees and the island it hailed from. Lizards from smaller islands with fewer types of predator, or that had been disconnected from mainland predators for longer, let her come far closer compared with their more fearful relatives (*Evolution*, doi.org/wv7).

In lab tests, Brock also found that lizards from safer islands were less likely to ditch their tails when put under physical pressure through pinching. "If you're living in a predator-free environment, it would be evolutionarily disadvantageous to spend your time running away while other lizards are foraging and mating," she says.

Printable transistor can tell what ails you

GOT a mystery bug? Printable plastic transistors that can directly detect pathogens in blood or saliva could one day tell tonsillitis from flu – in a flash.

Transistors easily switch on and off in response to an applied voltage, which allows electric current to flow between two terminals. But they can respond to other things as well, says Mariana Medina Sánchez, now at the Leibniz Institute for Solid State and Materials Research in Germany. She and her colleagues have engineered an inkjet-printable transistor that can recognise the protein biomarkers of common diseases, switching on only when it has detected them.

The team printed a transistor using a special ink embedded with a common antibody called human immunoglobulin G, which binds to antigens from a number of common viruses, bacteria and fungi. When a disease protein binds to an antibody, it changes the transistor's electrical properties, altering the voltage level at which it turns on (*Advanced Functional Materials*, doi.org/f2kdyz).

Eventually, the team says, doctors could print out a sheet of the devices – each equipped with a different disease antigen – and diagnose people in a snap.

Plants make their own sunscreen

THEY bask in the sun for hours, but just like us, plants need to protect themselves from damaging ultraviolet rays. Now we know how they do it.

Many plants use a group of chemicals called sinapate esters to defend against the sun while they absorb light for photosynthesis. These aromatic compounds sit in the upper cell layers of these plants' leaves and one type – sinapoyl malate – provides the bulk of this UV protection.

A team led by Timothy Zwier of Purdue University in West Lafayette, Indiana, has probed how sinapoyl malate works. They found that it filters out the entire spectrum of UV B radiation, which is known to damage plant and human DNA.

"It can absorb all wavelengths of UV B radiation, with no gaps in coverage," says Zwier, who says his finding could be useful for developing more resistant plants.

Giant galactic core in black hole battle

THE largest galactic core ever seen may be the remnant of a battle for black hole supremacy.

Omar Lopez-Cruz of Mexico's National Institute of Astrophysics, Optics and Electronics and his team measured the core of galaxy Holm 15A, 650 million light years from Earth. They found it was a record-breaking 15,000 light years across – about one-sixth the diameter of the entire Milky Way.

The core's size suggests the black hole it hosts could weigh 100 billion times the mass of our sun – nearly as much as the Milky Way (*Astrophysical Journal Letters*, doi.org/wkt). If so, it probably formed as two or three separate black holes jostled for position before merging into one, puffing up Holm 15A's core in the process.